Limited Feedback SVD Precoding for MIMO-OFDM systems

Dual Degree Project Report

submitted in partial fulfillment of the requirements
for the degree of

Bachelor & Master of Technology

by

Agrim Gupta
Roll No: 140020003

under the guidance of

Prof. Kumar Appaiah, Prof. Rahul Vaze

Department of Electrical Engineering

INDIAN INSTITUTE OF TECHNOLOGY BOMBAY

May 2018 - May 2019

Dissertation Approval Sheet

This is to certify that the dissertation titled

Limited Feedback SVD Precoding for MIMO-OFDM systems

by

Agrim Gupta
(140020003)

is approved for the degree of **Bachelor & Master of Technology** in
Electrical Engineering with a specialization in Communication and Signal Processing.

_____

Prof. Kumar Appaiah
(Guide)

_____

Internal Examiner

_____

External Examiner

_____

Chairperson

Date : 20/06/2019 _____

Declaration

I declare that this written submission represents my ideas in my own words and where others' ideas or words have been included, I have adequately cited and referenced the original sources. I declare that I have properly and accurately acknowledged all sources used in the production of this thesis. I also declare that I have adhered to all principles of academic honesty and integrity and have not misrepresented or fabricated or falsified any idea/data/fact/source in my submission. I understand that any violation of the above will be a cause for disciplinary action by the Institute and can also evoke penal action from the sources which have not been properly cited or from whom proper permission has not been taken when needed.

Date: June 20, 2019

Agrim Gupta

(Roll No: 140020003)

Acknowledgments

I would like to express my gratitude to my guide Prof. **Kumar Appaiah** and my co-guide Prof. **Rahul Vaze** for their guidance and support throughout the semester. The discussions with them were both illuminating and intellectually taxing. Particularly, I'm thankful to them for helping me improve my writing and presentation skills by providing me with critical inputs after countless careful reviews of my manuscripts.

I would also like to thank **Pranav Sankhe** (4-th year DD CSP student) and Prof. **Manoj Gopalakrishnan** for their help in the second stage of the project. It was while discussing the interplay of Machine Learning and Chaos Theory with Pranav (for Prof. Manoj's course project) when I got the idea of utilizing the reservoir computing framework for the purpose of predictive quantization of SVD precoders.

Agrim Gupta
IIT Bombay
June 20, 2019

Contents

Chapter 1

Predictive Quantization and Joint Time-Frequency Interpolation Technique for MIMO-OFDM Precoding*

Chapter Abstract

Precoding transmissions in wireless MIMO systems is essential to enable optimal utilization of the spatial degrees of freedom. However, communicating the precoding matrices to the transmitter from the receiver is challenging, owing to large feedback requirements. Past work has shown that predictive quantization in time, as well as interpolation over frequency can be used for effective feedback of the precoders. Moreover, interpolation strategies for MIMO systems where the number of antennas at the transmitter (N_T) is different from the number of antennas at the receiver (N_R), using the well known unitary group geodesic requires quantization of redundant information, thereby increasing feedback overheads. Our key contributions cover two aspects. First, we propose an efficient interpolation strategy for systems with $N_T \neq N_R$. Building upon this, we propose a predictive quantization as well as an interpolation strategy to exploit the available time-frequency correlations in the fed back precoders jointly. The key insight we use is that local tangent spaces in the underlying manifold structure of the precoder matrices permit effective combination of both temporal and frequency domain information for more accurate precoder reconstruction. Simulations reveal that by jointly exploiting the time-frequency correlations we obtain a significant improvement in achievable rate as well as BER reduction when compared to existing strategies which exploit the time-frequency correlations independently.

*This work has been presented at **IEEE ICC 2019** [1], and an extended journal version has been submitted to **IEEE Transactions on Communications**

1.1 Introduction

The use of orthogonal frequency division multiplexing (OFDM) with N subcarriers in multi-antenna ($N_T \times N_R$) wireless systems allows the treatment of a frequency-selective channel as a frequency-flat multiple-input multiple-output (MIMO) channel on a per subcarrier basis. This enables low-complexity receiver implementations, particularly for equalization. To maximally utilize the benefit of having MIMO antennas, the receiver needs to feed back channel state information (CSI) to the transmitter, which then uses it for precoding (matrix transformation of the input signal). Precoding enables efficient allocation of power across transmit antennas by waterfilling, and efficient signaling to increase rate while reducing bit-error-rate (BER) [2].

Modern wireless OFDM systems support thousands of subcarriers, thus the CSI requirement for precoding is rather large. However, only a certain number of subcarriers are reserved for CSI transmission in practice. Also, the receiver has to quantize these fed back matrices using just a few bits, due to the limited feedback constraint. Several standards consider the use of limited feedback to enhance system performance CITE. In the MIMO case, since these precoding matrices are high dimensional entities, quantizing them with few bits incurs substantial quantization error. The key challenge at the transmitter is to both estimate the precoding matrices at the non-fed back subcarriers via some interpolation algorithm, and to counter the substantial quantization error that arises due to quantization with just a few bits via a predictive quantization algorithm. This necessitates exploiting the correlations across frequency for interpolation algorithms [3] to estimate precoding matrices at subcarriers for which the receiver did not provide feedback. To address the quantization error issue, the transmitter requires the receiver to utilize the available correlations in the past fed back precoders and perform predictive quantization, instead of just independently quantizing the matrices for each OFDM frame separately. This enables lowering of quantization error with time and improves the performance of the MIMO system [4, 5].

One of the key challenges in designing the interpolation and predictive quantization algorithms is that the optimal precoding matrices for communication scenarios like waterfilling, ML receiver, MMSE/ZF linear receiver etc do not form a vector space, which renders linear algorithms for interpolation and predictive quantization ineffective. However, these matrices have an underlying manifold geometry [4–7], which can be exploited to design the required algorithms to interpolate and predict. A traditional method of obtaining the precoding matrix is to take the SVD of the channel matrix at the receiver and feed back the resulting quantized matrices which represent the directions and magnitudes of the channel eigenmodes, to the transmitter. Depending on the degrees of freedom that the transmitter has in allocating power to the N orthogonal streams (corresponding to total N subcarriers) emanating from its N_T transmit antennas, the optimal precoders to maximize the achievable rate reside either on the Grassmannian manifold or the Stiefel Manifold [4]. When the transmitter treats each channel eigenmode in the same manner, viz. doesn't discriminate between the strongest and weakest channel eigenmodes, the optimal precoders reside on the Grassmannian manifold, since the required information for the receiver to feed back to the transmitter constitutes of just the subspace formed by directions of the channel eigenmodes. When the receiver uses ML algorithm to decode the constellation points, the optimal precoders also reside on Grassmannian manifold [6].

However, the transmitter can also allocate the transmit power among the N orthogonal streams emanating from its N_T transmit antennas via waterfilling to prioritize the benefits offered by stronger eigenmodes. The receiver, in this case, needs to feed back the directions of the individual channel eigenmodes as well, and not only the subspace that they form. Hence, in the waterfilling case, the optimal precoders lie on the Stiefel manifold. In the waterfilling case, when $N_T = N_R$, the optimal precoders form unitary matrices and reside on the unitary group. When the receiver employs MMSE decoding of the constellation points, the optimal precoders reside on permutation invariant flag manifold [6] instead of the Stiefel manifold. The permutation invariant flag manifold is actually a lower dimensional manifold than the Stiefel manifold. However, when compared to Grassmannian manifold, the flag manifold provides more degrees of freedom, and hence it is a space in middle of Grassmannian and Stiefel when analyzing the manifold dimensions. In this paper, we consider two performance metrics of a point-to-point MIMO link, achievable rate obtained via optimal power allocation using waterfilling and BER using MMSE decoding. The optimal precoders for the former case, obtained via SVD of the channel matrix reside on the Stiefel Manifold. Since the Stiefel manifold has been studied more extensively than the Flag manifold, we pay a dimensional penalty and employ the Stiefel manifold precoders for the BER MMSE case as well. We capture the temporal, frequency correlations jointly to perform both predictive quantization and interpolation by utilizing the underlying Stiefel manifold structure.

Exploiting the manifold structure with local linear operations in the tangent space allows for algorithms to interpolate precoders at those subcarriers where feedback is not available at the transmitter. This also allows the receiver to improve upon the quantization error using predictive quantization methods. The most popular interpolation strategy for unitary precoders is the Geodesic scheme [3], which interpolates across two fed back unitary precoding matrices by joining them with the shortest path between them, and splitting the path into equal sections to obtain precoders at subcarriers where feedback is unavailable. Although not very explicit, this scheme also uses the linearity of the local tangent space. The role of local linear tangent spaces is more explicit in [4, 5], both of which first utilize the tangent spaces to make predictions for the new precoders at both the transmitter and the receiver, and then capture the channel innovation by quantizing the tangent space near the obtained prediction at the receiver. The reciever then feeds back the quantized direction in the tangent space to the transmitter so that the transmitter obtains a refined estimate for the new precoder from the predicted precoder.

Several past approaches have largely exploited frequency or temporal correlation in isolation for interpolation and prediction [4, 5, 8–13]. For the case where the precoding matrix is not square ($N_T \neq N_R$), temporal correlation has been used in [4] and an interpolation algorithm has been suggested in [7]. A non-manifold based approach to simultaneously capture frequency and temporal correlation is presented in [14]. Capturing time-frequency correlations jointly for adaptive quantization on the Grassmanian manifold for the MISO communication setting has been presented in [15]. Past work that has considered utilizing the manifold structure for interpolation algorithms has largely been concerned with unitary group [3, 10], where the algorithms are implemented over the full $N_T \times N_T$ unitary space. When $N_T > N_R$, the effective dimensions are given by $N_T \times N_R$ matrices residing in the Stiefel manifold. Therefore, algorithms for limited feedback that

operate over the complete unitary space are redundant. When $N_T \neq N_R$, operating over the Stiefel manifold, allows working with the effective dimensions of the optimal precoder matrices, thereby reducing the CSI overhead. However computing explicit geodesics over the Stiefel manifold is challenging [16, 17]. In recent work, a Lloyd type codebook scheme has been suggested for direct quantization of matrices residing in the Stiefel manifold [18], and it has been shown that explicit quasi-geodesics can be computed over the Stiefel manifold using the Cayley exponential lifting-retraction pair [19]. We exploit both of these recent results to reduce the overhead requirement by quantizing at the receiver and interpolating at the transmitter, both while working with the effective dimensions of the Stiefel manifold.

In addition to working with the Stiefel manifold quasi-geodesics, we also focus on jointly exploiting the temporal and the frequency correlation for efficient limited CSI feedback. To the best of our knowledge, prior work has considered quantization over the Stiefel manifold only in the presence of temporal correlations [4], or in the frequency domain [7], but not jointly. Exploiting temporal and frequency correlation presents novel challenges, and we propose a predictive quantization and interpolation strategy that can be implemented over the Stiefel manifold, that builds upon the ideas presented in [4, 11, 15]. The novel idea here is that the local tangent space, in addition to offering linearity for easier mathematical modeling, also allows for effective combination of both temporal and frequency domain information (Also suggested for the MISO Grammanian scenario in [15]), available in the past precoding matrices fed back to the transmitter. This allows for much better utilization of the limited feedback obtained in the past, for more effective quantization and interpolation, thereby significantly improving the system performance.

We provide extensive simulations to illustrate the benefits of our approach in terms of improving the BER, the achievable rate and channel estimation error (measured via the chordal metric). Our simulations for various mobility conditions as well as different wireless channel profiles reveal that, using 6 bits per fed back precoder for the 4×2 MIMO channel, we are able to reduce the E_b/N_0 requirement by around $\sim$ 3 dB for the same BER, when compared to the earlier temporal prediction based approaches. In addition, the achievable rate we obtain using our limited feedback scheme is close to 95% of the rate achievable using perfect precoder knowledge for each subcarrier at the transmitter.

The following points were covered in this paper and not in the conference version [1]:

1. Detailed solution of the optimization problem proposed for obtaining unit step tangent matrices $\mathcal{T}_{i,t}, \mathcal{F}_{i,t}$, along with a complete description of the lifting/retraction maps used.

2. Evaluation of the presented algorithm for joint time-frequency interpolation and predictive quantization on the channels generated in accordance with the ITU Pedestrian Channel model, with 64 subcarriers

3. Achievable rate results for the proposed interpolation scheme on the Stiefel Manifold utilizing the Cayley exponential maps

The rest of the paper is organized as follows. Section 1.2 describes the system model and SVD based precoding schemes. Section 1.3 elaborates on interpolation directly on the Stiefel Manifold via the Cayley lifting map. We present a frequency hopping strategy,

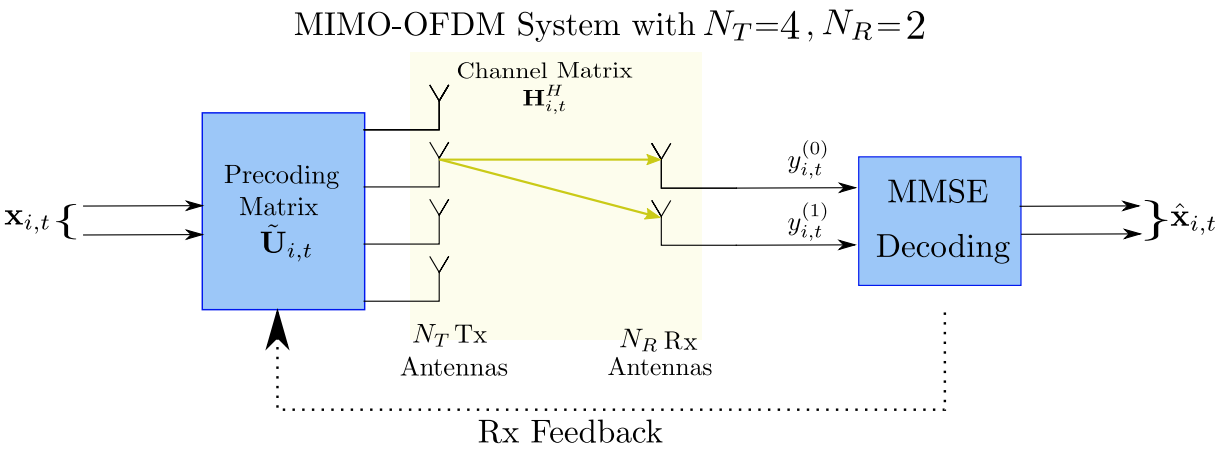

Figure 1.1: Sample point-to-point MIMO-OFDM setting that we consider, with unequal number of transmit and receive antennas. The system shown is a 4×2 system, where the precoding matrix $\tilde{\mathbf{U}}_{i,t}$ is a 4×2 with $\tilde{\mathbf{U}}_{i,t}^H \tilde{\mathbf{U}}_{i,t} = \mathbf{I}_2$. Channel estimates at the receiver are used to feed back $\tilde{\mathbf{U}}_{i,t}$ to the transmitter.

predictive quantization technique and joint time-frequency interpolation scheme for precoders on the Stiefel manifold in Section 1.4. Section 1.5 presents the simulation results and finally Section 1.6 concludes.

1.2 System Model

We consider a point-to-point MIMO-OFDM wireless system that has N_T transmit antennas and N_R receive antennas. The available bandwidth is divided into N subcarriers such that each subcarrier has a nearly flat frequency response, as is commonly the case in the OFDM systems. The transmitter communicates an $N_s \times 1$ data vector, where $N_s \leq \min(N_T, N_R)$, and the $N_T \times N_s$ precoding matrix maps the $N_s \times 1$ data vector onto the $N_T \times 1$ transmit vector emanating out of the transmitter. In this discussion, we assume that $N_T > N_R$ and $N_s = N_R$. Keeping notations consistent with [4], the $N_R \times 1$ data stream received is denoted by

$$\mathbf{y}_{i,t} = \mathbf{H}_{i,t}^H \tilde{\mathbf{U}}_{i,t} \mathbf{x}_{i,t} + \mathbf{w}_{i,t}$$

where $\tilde{\mathbf{U}}_{i,t} \in \mathbb{C}^{N_T \times N_R}$ denotes the precoding matrix used by the transmitter, which is a function of quantized channel information fed back by the receiver, $\mathbf{y}_{i,t} \in \mathbb{C}^{N_R \times 1}$ is the received data stream, $\mathbf{x}_{i,t} \in \mathbb{C}^{N_R \times 1}$ denotes the transmitted signal at the i-th subcarrier ($i \in [0, \ldots N-1]$), of the t-th OFDM frame, $\mathbf{H}_{i,t} \in \mathbb{C}^{N_T \times N_R}$ denotes the MIMO channel matrix and $\mathbf{w}_{i,t}$ denotes the i.i.d. complex Gaussian noise with $\mathbf{w}_{i,t} \sim \mathcal{N}_{\mathbb{C}}(0, N_0 \mathbf{I}_{N_R})$ (N_0 is the noise variance). Using a MMSE decoder and the received $\mathbf{y}_{i,t}$, one obtains an estimate of $\mathbf{x}_{i,t}$, denoted by $\hat{\mathbf{x}}_{i,t}$. The system block diagram is presented in in Fig. 1.1.

We assume that the channel matrices $\mathbf{H}_{i,t}$ are estimated at the receiver exactly. If the exact channel matrices $\mathbf{H}_{i,t}$ are somehow made available at the transmitter, the optimal policy at the transmitter is to use the right singular vectors of $\mathbf{H}_{i,t}^H$ as the precoding matrices $\tilde{\mathbf{U}}_{i,t}$ to maximise the achievable rate. In particular, when we take the compact SVD of $\mathbf{H}_{i,t}$, we get,

$$\mathbf{H}_{i,t} = \mathbf{U}_{i,t} \Sigma_{i,t} \mathbf{V}_{i,t}, \tag{1.1}$$

and we have $\tilde{\mathbf{U}}_{i,t} = \mathbf{U}_{i,t}$. Since $\mathbf{U}_{i,t}$ is a lower dimensional entity than $\mathbf{H}_{i,t}$, it makes sense for the receiver to quantize and feed back $\mathbf{U}_{i,t}$ instead of $\mathbf{H}_{i,t}$, without losing out on the feedback benefits. Notice that the matrices $\mathbf{U}_{i,t}$ reside on the Stiefel manifold $\mathrm{St}(N_T, N_R)$, since the columns of $\mathbf{U}_{i,t}$ form a set of N_R orthogonal vectors in N_T dimensions. Given practical limitations, only limited feedback is available from the receiver, and the objective is to find 'reasonable' estimate of $\mathbf{U}_{i,t}$ at the transmitter, given by $\tilde{\mathbf{U}}_{i,t}$ using the available feedback bits.

Before proceeding, we discuss the geometry of the Stiefel manifold. The (compact) Stiefel manifold, $\mathrm{St}(m, n)$ represents the set of all ordered m orthogonal vectors in the vector space $\mathbb{C}^n$ [4]:

$$\mathrm{St}(m, n) = \{\mathbf{U} \in \mathbb{C}^{n \times m} | \mathbf{U}^H \mathbf{U} = \mathbf{I}_m\}.$$

$\mathrm{St}(m, n)$ does not form a vector space, because of which linear algorithms to interpolate and quantize are not effective, as these operations will result in violation of the $\mathbf{U}^H\mathbf{U} = \mathbf{I}_m$ constraint. That is, to interpolate between $\mathbf{A}$ and $\mathbf{B}$, with $\mathbf{A}, \mathbf{B} \in \mathrm{St}(m, n)$, evaluating $\lambda\mathbf{A} + (1 - \lambda)\mathbf{B}$, $\lambda \in (0, 1)$ yields a result that does not necessarily belong to $\mathrm{St}(m, n)$. Similarly, one can not use a linear prediction approach for predictive quantization. However, the tangent space local to a point $\mathbf{U} \in \mathrm{St}(m, n)$, defined as, $T_{\mathbf{U}}\mathrm{St}(m, n)$, forms a linear vector space that admits linear operations. The vector space property of the local tangent space facilitates prediction and interpolation algorithms for SVD precoders in the MIMO-OFDM setting.

We represent the considered limited feedback scenario by a time-frequency bins matrix (Fig. 1.2), where the t-th row and the i-th column corresponds to the precoding matrix at the t-th OFDM frame and the i-th subcarrier. The matrix is sparsely fed back (in terms of number of bins fed back) by the receiver to the transmitter, respecting the limited feedback constraint. The transmitter reconstructs the time-frequency bins matrix at non-fed back entries, by utilizing the temporal and frequency correlations of the nearby fed back points. The metric we choose to quantify the closeness of a reconstruction of the time-frequency bins matrix at the transmitter to the exact time-frequency bins matrix observed at the receiver is $d[t] = \frac{1}{N}\sum_{i=0}^{N-1} d_s(\tilde{\mathbf{U}}_{i,t}, \mathbf{U}_{i,t})$, with d_s being the chordal metric between two points in Stiefel manifold, defined as,

$$d_s(\mathbf{A}, \mathbf{B}) = \sqrt{\sum_{j=1}^{N_R} d_g^2(\mathbf{a}_j, \mathbf{b}_j)}, \;\; d_g(\mathbf{u}, \mathbf{v}) = \sqrt{1 - |\mathbf{u}^*\mathbf{v}|^2}, \tag{1.2}$$

where $\mathbf{A}, \mathbf{B} \in \mathrm{St}(N_T, N_R)$, and $\mathbf{a}_j, \mathbf{b}_j$ are the j-th columns of $\mathbf{A}$, $\mathbf{B}$ respectively, and $d_g(\mathbf{a}_j, \mathbf{b}_j)$ is the Grassmannian chordal distance between $\mathbf{a}_j$ and $\mathbf{b}_j$ [20]. Note here that d_s is actually not a distance metric on the Stiefel manifold, since $d_s(\mathbf{A}, -\mathbf{A}) = 0$, $\forall \mathbf{a} \in \mathrm{St}(N_T, N_R)$. However, it is still a suitable metric for error comaprison since the precoders are nicely correlated and the π phase shifts in SVD order has been corrected for manually while simulating (see Section 1.5 for more details). Observe that $d[t_1]$ at a particular time t_1 represents the average chordal metric over the N subcarriers, between the estimates and actual values of row t_1 in the time-frequency bins matrix. Thus, the objective is to come up with a strategy to reconstruct the sparsely fed back time-frequency bin matrix to minimize the chordal metric $d[t]$ and bring the performance as close to complete exact (i.e accurate unquantized precoding matrix available at each bin) time-frequency bins matrix.

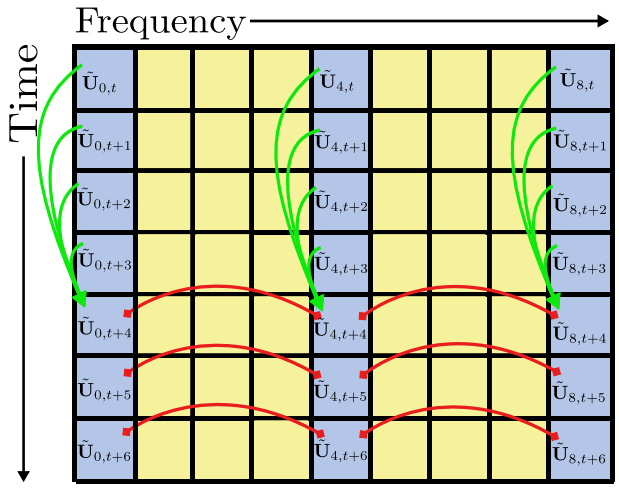

Figure 1.2: Exploiting regularly spaced limited feedback scheme for $N = 9$, with (yellow) blue cells indicating the (non) fed back indices. Frequency correlations are captured via the red interpolating curves, and the temporal correlations are used to improve the quantization over time (shown implicitly via green arrows).

With the sparsely fed back time-frequency bins matrix from the receiver, and the individual fed back precoders incurring substantial quantization errors, exploiting time and frequency correlations is absolutely imperative for reducing $d[t]$. Independently utilizing the temporal and frequency correlations to reconstruct the time-frequency bins matrix at the transmitter can be performed using a frequency based interpolation scheme, coupled with a time based predictive quantization scheme. We use the prior work on predictive quantization over $\mathrm{St}(N_T, N_R)$ [4] and the interpolation scheme suggested over $\mathrm{St}(N_T, N_R)$ in Section 1.3, to reconstruct the time-frequency bin matrix using the strategy shown in Fig. 1.2, by sending feedback on regularly spaced subcarrier indices. The strategy depicted in Fig. 1.2 forms a baseline of comparison for our proposed scheme which exploits time-frequency correlations jointly.

Our proposed joint frequency-time scheme is aided by a hopping strategy (Section 1.4), where the locations of fed back subcarriers are alternated with time. With the use of the hopping scheme, we effectively combine both temporal and frequency domain information in the tangent spaces of the Stiefel manifold, on which the precoders $\tilde{\mathbf{U}}_{i,t}$ lie (Section 1.4.1). With the predictive quantization scheme at the receiver, we show that the quantization chordal metric ($d_s(\tilde{\mathbf{U}}_{i,t}, \mathbf{U}_{i,t})$) decreases as t increases, viz. the receiver feeds back refined estimates of each row of time-frequency bins matrix in subsequent OFDM frame. In addition, we also propose a joint time-frequency interpolation scheme (Section 1.4.3) at the transmitter, to reconstruct the precoders at the missing subcarriers in every OFDM frame by effectively using the refined fed back precoders at the transmitter. We empirically show that jointly exploiting the frequency and temporal correlations improves $d[t]$ metric as compared to the independent utilization of the said correlations, which in turn allows for lower BER and higher achievable rate.

1.3 Proposed Interpolation on $St(N_T, N_R)$

In this section, we describe the limited feedback scheme that allows reconstruction of time-frequency bins matrix at the transmitter by exploiting the temporal and frequency

correlations independently. To exploit temporal correlations, we utilize the past work in [4], which described a predictive quantization scheme on the Stiefel manifold, although that was limited only to a flat fading channel. A natural approach to exploit frequency correlations by interpolating, would be to use geodesics, but true geodesic curves with explicit solutions in the Stiefel manifold are not straightforward [7, 16, 17]. Recently, [19] has proposed a unique quasi-geodesic curve using the Cayley type lifting-retraction maps that enable direct interpolation on $\mathrm{St}(N_T, N_R)$, which we utilize in our proposed interpolation scheme. Interpolation directly on $\mathrm{St}(N_T, N_R)$ has been discussed only in [7], albeit for unquantized precoders. An alternate approach towards interpolating on Stiefel manifold would be to project the matrix residing in the Stiefel manifold to the unitary group, then use the well known $\{\mathrm{expm}(\cdot) - \mathrm{logm}(\cdot)\}$ geodesic curve, and finally project the unitary matrix back to the Stiefel manifold. Simulations reveal that quantization plays a key role in performance comparison of the proposed interpolation scheme on Stiefel manifold versus interpolating on the unitary group.

In order to obtain a unitary precoding matrix, we take the full SVD of MIMO channel matrix observed at the receiver, instead of a compact SVD. The full SVD of $\mathbf{H}_{i,t}$ yields $\boldsymbol{\mathcal{U}}_{i,t}\boldsymbol{\Sigma}_{i,t}\mathbf{V}_{i,t}$, where $\boldsymbol{\mathcal{U}}_{i,t} \in \mathbb{C}^{N_T \times N_T}$ is a unitary matrix, $\Sigma_{i,t} \in \mathbb{C}^{N_T \times N_R}$ is a diagonal matrix, and $\mathbf{V}_{i,t} \in \mathbb{C}^{N_R \times N_R}$ is a unitary matrix. The optimal precoder consists of the first N_R columns of $\boldsymbol{\mathcal{U}}_{i,t}$ [3]. Selecting the first N_R rows projects the unitary matrix back onto the Stiefel manifold. We represent $\tilde{\boldsymbol{\mathcal{U}}}_{i,t}$, as the matrix ultimately used by transmitter for precoding (and interpolating across non-fed back points), which is obtained by quantizing $\boldsymbol{\mathcal{U}}_{i,t}$. The usual approach using geodesic interpolation on the unitary group is as follows. Let us suppose that $\tilde{\boldsymbol{\mathcal{U}}}_{i,t}$ have been fed back for subcarriers i_1 and i_2, $i_1 < i_2$. The transmitter interpolates the precoding matrix at i-th subcarrier, with $i_1 < i < i_2$ using the geodesic scheme in (1.3)

$$\tilde{\boldsymbol{\mathcal{U}}}_{i,t} = \tilde{\boldsymbol{\mathcal{U}}}_{i_1,t}\mathrm{expm}\left(\frac{i - i_1}{i_2 - i_1}\mathrm{logm}(\tilde{\boldsymbol{\mathcal{U}}}_{i_1,t}^{-1}\tilde{\boldsymbol{\mathcal{U}}}_{i_2,t})\right), \tag{1.3}$$

where expm and logm refer to the matrix exponential and matrix logarithm, respectively. The precoding matrices are then obtained by taking the first N_R columns of the $\tilde{\boldsymbol{\mathcal{U}}}_{i,t}$ matrices obtained after interpolation, since we require only the first N_R right singular vectors. The remaining $N_T - N_R$ columns, which were included in the precoding matrix to form a unitary matrix and enable interpolation with geodesics, are actually redundant. Quantization with this redundant information would incur allocation of bits for unneeded information.

We now propose a method to directly interpolate over the Stiefel manifold, thereby obviating the need to quantize the redundant information. Let us suppose that $\tilde{\mathbf{U}}_{i,t}$ have been fed back for subcarriers i_1 and i_2, $i_1 < i_2$. We propose an interpolation method using the Cayley exponential lifting and retraction maps at $\tilde{\mathbf{U}}_{i_i,t}$, denoted as $\mathrm{Exp}^{-1}_{\tilde{\mathbf{U}}_{i_1,t}}(\cdot)$ and $\mathrm{Exp}_{\tilde{\mathbf{U}}_{i_1,t}}(\cdot)$ respectively (for explicit definitions refer Appendix Section 1.7.1), consistent with the notation in [19]. The transmitter interpolates the precoding matrix at i-th subcarrier, with $i_1 < i < i_2$ using (1.4)

$$\tilde{\mathbf{U}}_{i,t} = \mathrm{Exp}_{\tilde{\mathbf{U}}_{i_1,t}}\left(\frac{i - i_1}{i_2 - i_1}\mathrm{Exp}^{-1}_{\tilde{\mathbf{U}}_{i_1,t}}\left(\tilde{\mathbf{U}}_{i_2,t}\right)\right). \tag{1.4}$$

One thing to note is that the $\mathrm{logm}(\cdot)$ maps $N_T \times N_T$ unitary matrices to $N_T \times N_T$ skew-

Hermitian matrices. Similarly, the $\text{Exp}^{-1}(\cdot)$ in Equation 1.4 maps $N_T \times N_R$ matrices on $\text{St}(N_T, N_R)$ to $N_T \times N_T$ skew-Hermitian matrices, with the lower right $(N_T - N_R) \times (N_T - N_R)$ minor being the null matrix. A more detailed treatment is available in Appendix Section 1.7.1.

Using the approach described in (1.4), the receiver needs to quantize and feed back only the $N_T \times N_R$ matrices $\mathbf{U}_{i,t}$, with $\mathbf{U}_{i,t}^H \mathbf{U}_{i,t} = \mathbf{I}_{N_R}$ instead of $N_T \times N_T$ unitary matrices $\boldsymbol{\mathcal{U}}_{i,t}$, thereby obviating the need to quantize redundant information by working in lower dimensionsal Stiefel manifold. Improvement in performance (BER and achievable rate) stemming from interpolation in reduced dimensions is quantified by our simulations in Section 1.5.

Before concluding this section, we summarize the presented work till now and its connection with the upcoming sections. Our novel contribution in this section is the Cayley interpolation method over the Stiefel manifold, which utilizes recently proposed Cayley exponential lifting-retraction pairs presented in [19]. An alternate method of interpolating on the Stiefel manifold would be to utilize the unitary group geodesic, by projecting matrices in the Stiefel manifold to and fro onto the unitary group. Section 1.5.1 empirically illustrates the performance benefits of the proposed Cayley interpolation over unitary group geodesic interpolation. Using the proposed Cayley interpolation method and the predictive quantization algorithm presented in [4] for flat fading channel, the time-frequency bins matrix can be populated as shown in Fig. 1.2. The strategy in Fig. 1.2 utilizes the temporal and frequency correlations independently to quantize the precoders at feed back bins and interpolate the precoders at non fed back bins. The upcoming section would elaborate upon a different strategy to perform the same (Fig. 1.3, 1.5). The key difference is that the scheme presented in Section 1.4 utilizes the joint time-frequency correlations to perform both predictive quantization and interpolations. In Section 1.5 it is empirically shown that the capturing joint correlations is indeed fruitful and brings about significant performance gains.

1.4 Predictive Quantization and Joint Time-Frequency Interpolation

In this section, we describe a predictive quantization method employed by the receiver, coupled with an interpolation scheme at the transmitter to exploit both the temporal and the frequency correlations, which enables more efficient reconstruction of the time-frequency bins matrix with a lower $d[t]$ metric and improved performance (BER and achievable rate).

We first propose a hopping feed back strategy (Fig. 1.3), instead of feeding back precoding matrices at regularly spaced subcarriers (Fig. 1.2). In the hopping strategy, the fed back precoding matrices' bins in the time-frequency bins matrix alternate with each OFDM frame. The hopping strategy allows the receiver to exploit joint time-frequency correlations for improved predictive quantization, enabling feedback to the transmitter with lower quantization error. The transmitter gets feedback with reduced quantization error, at time-alternated frequency positions in the time-frequency bins matrix, which it then uses to reconstruct the matrices at non fed-back entries of the time-frequency bins

matrix, using the proposed joint time-frequency interpolation scheme. Hence, our proposed scheme improves upon both the aspects of the limited feedback precoding scheme, viz. the predictive quantization at the receiver and interpolation algorithm at the transmitter. This allows for more efficient utilization of the bits allocated for feed back of precoding matrices, as compared to the scheme in Fig. 1.2, which exploited temporal and frequency correlations independently instead of doing it jointly. This section describes the explicit details pertaining to both of these proposed methods.

1.4.1 Hopping and Prediction Scheme

The approach for interpolation and prediction, shown in Fig. 1.2 feeds back precoders only at a fixed set of equally spaced out subcarriers, and the remaining subcarriers' precoders are interpolated. This method has two disadvantages. One is that the precoders for those subcarriers that lie in the middle of the fed back subcarriers, face larger interpolation errors, since they are equally far from the fed back subcarriers. The other is that, when predictively quantizing solely over the time-domain, we ignore the useful past information present in the nearby subcarriers due to frequency correlations. We therefore suggest a "hopping" scheme, in which the fed back frequency bins alternate with each OFDM frame, to improve upon both the interpolation and quantization errors as compared to the scheme in Fig. 1.2.

We now describe our hopping strategy both mathematically and using a visual illustration (Fig. 1.3). Let D_f be the frequency separation between two precoders estimated at the receiver, and δ_f be the frequency offset of the hopping scheme, both measured in terms of number of subcarriers (depicted in Fig. 1.3). We choose D_f as a factor of $N-1$, where N is the total number of subcarriers. We alternate between feeding back the precoder at subcarriers $\{mD_f | m = 0, 1, 2, \ldots (N-1)/D_f\}$ in one OFDM frame and subcarriers $\{\delta_f + mD_f | m = 0, 1, 2, \ldots (N-1)/D_f - 1\}$ in the next OFDM frame. We set $\delta_f = \lfloor D_f/2 \rfloor$ to address the issue of large interpolation errors in the middle of two fed back precoders. This permits us to obtain a more accurate reconstruction of the precoder variation across frequency due to reduced interpolation error. The hopping strategy is visually illustrated in Fig. 1.3. The yellow boxes in Fig. 1.3 indicate the time-frequency bins for which the quantized $\tilde{\mathbf{U}}_{i,t} \in \mathrm{St}(N_T, N_R)$ were fed back. The white boxes in the same figure indicate the time-frequency bins for which the precoding matrices were not fed back. In the subsequent discussions, we refer to the value of the precoding matrix at subcarrier i at time t, viz. $\tilde{\mathbf{U}}_{i,t}$, merely by referring to it as the precoder at box (i, t).

We now present our proposed predictive quantization scheme which exploits the joint time-frequency correlations arising out from the hopping feedback strategy. For the t-th OFDM frame, i-th subcarrier, the transmitter uses the past fed back information to obtain a prediction, say $\mathbf{P}_{i,t}$ for those boxes where the receiver would provide feedback in the next time frame. This situation is depicted in Fig. 1.3 for the $(t+6)$-th OFDM frame. The feedback from the receiver indicates the quantized direction in the local tangent space of $\mathbf{P}_{i,t}$, going along which transmitter obtains the precoder estimate $\tilde{\mathbf{U}}_{i,t}$ closest in terms of chordal metric to the actual precoder $\mathbf{U}_{i,t}$. The feedback helps transmitter capture channel innovation (viz. difference between predicted precoder and actual precoder), whereas the prediction utilizes the joint time-frequency correlations to minimize the innovation feedback required (viz. reduce the chordal metric as far as possible between the predicted

and actual precoder).

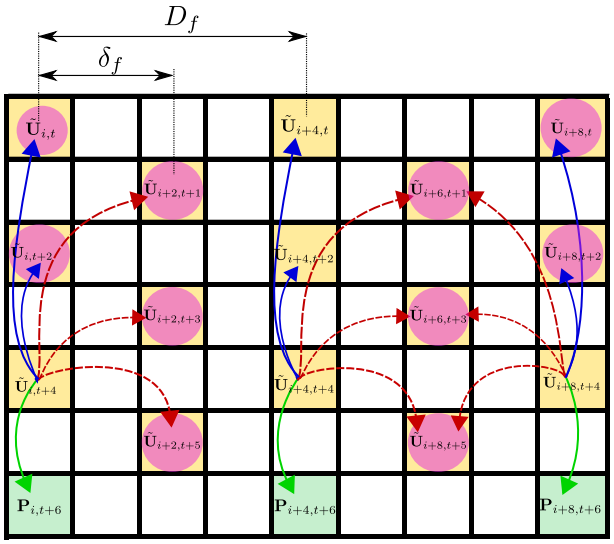

Figure 1.3: Hopping strategy for $N = 9, D_f = 4, \delta_f = 2$. The red, blue and green curves represent the tangents on $\mathrm{St}(N_T, N_R)$, illustrated in Fig. 1.4.

For prediction, we use a lifting map to obtain local tangent spaces, optimize linear functions in the local tangent spaces, and then finally use a retraction map that corresponds to the chosen lifting map to return to the manifold. We obtain the tangent from box (i,t) to nearby box (j,s), denoted as $\mathbf{T}_{i,t}^{j,s}$, viz. the tangent emanating from $\tilde{\mathbf{U}}_{i,t}$ to $\tilde{\mathbf{U}}_{j,s}$ using the chosen lifting operation, denoted by $\mathbf{T}_{i,t}^{j,s} = \mathtt{lift}_{\tilde{\mathbf{U}}_{i,t}}\left(\tilde{\mathbf{U}}_{j,s}\right)$. The corresponding retraction operation to return back to the manifold is given by $\mathtt{retract}_{\tilde{\mathbf{U}}_{i,t}}\left(\mathbf{T}_{i,t}^{j,s}\right)$. Since the local tangent space forms a vector space, $\mathbf{T}_{i,t}^{j,s}$ can be approximated by a linear combination of two matrices that represent the unit tangent matrices in time and frequency domain separately, local to (i,t). That is, going along $\mathcal{F}_{i,t}$ from $\tilde{\mathbf{U}}_{i,t}$, gives an estimate of $\tilde{\mathbf{U}}_{i+1,t}$, and similarly, going along $\mathcal{T}_{i,t}$ from $\tilde{\mathbf{U}}_{i,t}$, gives an estimate of $\tilde{\mathbf{U}}_{i,t+1}$. In other words, there exist matrices $\mathcal{T}_{i,t}, \mathcal{F}_{i,t}$ such that $\mathbf{T}_{i,t}^{j,s} \approx \mathcal{F}_{i,t}\Delta f + \mathcal{T}_{i,t}\Delta t$, where $\Delta f, \Delta t \in \mathbb{Z}$ are steps in the time and frequency axes respectively, i.e. $\Delta f = j - i$ and $\Delta t = s - t$, the signed frequency/time separation between boxes (j,t) and (i,t). This construct allows us to effectively combine information from temporal and frequency correlations in the local tangent space (similar to discussions in [5]), captured by $\mathcal{T}_{i,t}$ and $\mathcal{F}_{i,t}$ respectively. We estimate $\mathcal{F}_{i,t}, \mathcal{T}_{i,t}$ using a least-squares fit over the known tangents to $(j,s) \in \mathtt{nbrs}_{i,t}(p)$. $\mathtt{nbrs}_{i,t}(p)$ (defined below) refers to the collection of p past neighbours of (i,t), which are lifted to the tangent space local to i,t for estimating $\mathcal{F}_{i,t}, \mathcal{T}_{i,t}$. Let,

$$\mathtt{same\_freq\_nbrs}_{i,t}(p) = \{(i, t-2m) | m \in \{1 \dots p-1\}\}, \text{ and,}$$
$$\mathtt{diff\_freq\_nbrs}_{i,t}(p,q) = \{(i + q\delta_f, t-2m+1) | m \in \{1 \dots p\}\}$$

where $q = +1/-1$ indicates right/left neighbors. To estimate $\mathcal{F}_{i,t}, \mathcal{T}_{i,t}$, we require to invert a matrix $\mathbf{\Delta}_{i,t}$ (1.7),(1.8). To ensure that $\mathbf{\Delta}_{i,t}$ is invertible, we take frequency separations only on one side, which gives,

$$\mathtt{nbrs}_{i,t}(p) = \begin{cases} \mathtt{same\_freq\_nbrs}_{i,t}(p) \bigcup \mathtt{diff\_freq\_nbrs}_{i,t}(p,1), & \text{for } i \neq N-1 \\ \mathtt{same\_freq\_nbrs}_{i,t}(p) \bigcup \mathtt{diff\_freq\_nbrs}_{i,t}(p,-1), & \text{for } i = N-1 \end{cases} \tag{1.5}$$

where N is the total number of subcarriers, indexed from 0. In Fig. 1.3, the purple encircled boxes represent $\texttt{nbrs}_{i,t+4}(3)$ and $\texttt{nbrs}_{i+8,t+4}(3)$ respectively. With the neighbouring precoders defined, we frame the following objective function to estimate $\mathcal{F}_{i,t}, \mathcal{T}_{i,t}$,

$$\mathcal{F}_{i,t}, \mathcal{T}_{i,t} \leftarrow \text{argmin}_{\mathsf{F}_{i,t}, \mathsf{T}_{i,t}} \sum_{(j,s)\in \texttt{nbrs}_{i,t}(p)} ||(\mathsf{F}_{i,t}(j-i) + \mathsf{T}_{i,t}(s-t) - \mathbf{T}_{i,t}^{j,s})||_F^2 \tag{1.6}$$

where $||\cdot||_F$ represents Frobenius norm. We take partial derivatives of the objective function in (1.6) with respect to $\mathcal{F}_{i,t}, \mathcal{T}_{i,t}$ and set them to be the null matrix (for a detailed proof of the below equations, refer Appendix Section 1.7.2) to get the following expressions for $\mathcal{F}_{i,t}, \mathcal{T}_{i,t}$ after optimizing the objective function:

$$\begin{bmatrix} \mathcal{F}_{i,t} \\ \mathcal{T}_{i,t} \end{bmatrix} = \mathbf{\Delta}_{i,t}^{-1} \begin{bmatrix} \Sigma_{j,s}(j-i)\mathbf{T}_{i,t}^{j,s} \\ \Sigma_{j,s}(s-t)\mathbf{T}_{i,t}^{j,s} \end{bmatrix} \tag{1.7}$$

$$\mathbf{\Delta}_{i,t} = \begin{bmatrix} \Sigma_{j,s}(j-i)^2 & \Sigma_{j,s}(j-i)(s-t) \\ \Sigma_{j,s}(j-i)(s-t) & \Sigma_{j,s}(s-t)^2 \end{bmatrix} \tag{1.8}$$

As an example, consider how to predict the precoding matrix at box (k,l): When the temporal correlation of the channel is higher than the frequency correlation (measured in terms of chordal metric to exact precoder at the receiver), $(i,t) = (k, l-2)$, and if the frequency correlation is larger, $(i,t) = (k \pm 2, l-1)$. The transmitter would require additional feedback of 1 bit to indicate if the channel is correlated more nicely along frequency than along time. Also, the receiver need not send this feedback at each time instant, since this property of having nicer correlations along time/frequency would stick for a long enough time (given the quasi-stationary property of channel). Hence, we expect the net additional feedback amortized over time to be minimal. The chosen (i,t) is likely to be the closest among the past fed back points, in terms of chordal metric, to the new box (k,l).

The chosen (i,t) is referred to as the center (anchor point) on whose local tangent space we optimize to obtain $\mathcal{F}_{i,t}, \mathcal{T}_{i,t}$ using the known neighbouring boxes (j,s) around the center (i,t). We thus obtain the predicted precoder at box (k,l) given by $\mathbf{P}_{k,l} = \text{retract}(\tilde{\mathbf{U}}_{i,t}, \mathcal{F}_{i,t}(k-i) + \mathcal{T}_{i,t}(l-t))$. $\mathbf{P}_{k,l}$ is the outcome of the predictive quantization algorithm for box (k,l). Note that these operations can be performed at the transmitter independently without any additional feedback.

1.4.2 Quantization scheme

Having described the proposed prediction approach, we now describe the feed back approach. The feed back from the receiver signals the channel innovation, which the transmitter uses to obtain a refined estimate of the precoder from the prediction (which was the coarse estimate that the transmitter had without any additional feedback). Once we obtain the prediction $\mathbf{P}_{k,l}$, the receiver quantizes the tangent space local to $\mathbf{P}_{k,l}$ using a $\mathcal{B}$ bit codebook and feeds back the optimal index, which the transmitter utilizes to obtain the matrix $\tilde{\mathbf{U}}_{k,l}$, which is ultimately used for precoding. The approach used by us to quantize the tangent space local to the prediction is based on previous work for the same in [4, 5]. A codebook quantizing the local tangent space would have two components,

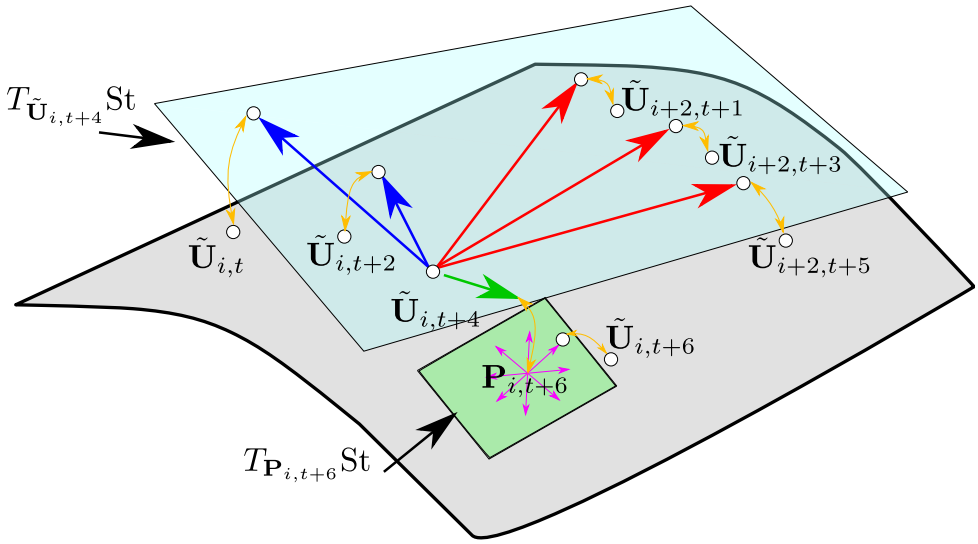

Figure 1.4: Predictive Quantization algorithm to obtain $\tilde{\mathbf{U}}_{i,t+6}$, with closest previous value being $\tilde{\mathbf{U}}_{i,t+4}$. The yellow curves represent the lifting/retraction operations. $\mathbf{P}_{i,t+6}$ is the predicted value of $\tilde{\mathbf{U}}_{i,t+6}$. The blue and green planes are the tangent spaces local to $\tilde{\mathbf{U}}_{i,t+4}$ and $\mathbf{P}_{i,t+6}$ respectively. The local tangent space at $\mathbf{P}_{i,t+6}$ is then quantized and fed back to obtain $\tilde{\mathbf{U}}_{i,t+6}$.

quantization of the directions in the tangent space, and quantization of magnitudes of steps taken in the quantized directions. We adopt the strategy in [4], which controls the magnitude of tangent steps, by having two codebooks T_p^C, T_m^C of different spreads, but same $2^{\mathcal{B}-1}$ base vectors $\in T_{\mathbf{P}_{k,l}}\mathrm{St}(N_T, N_R)$. The base vectors correspond to a collection of $2^{\mathcal{B}-1}$ vectors which represent the quantized directions. This collection is referred to as the base codebook $\mathcal{T}^B$ hereafter. By spread of codewords, we mean the volume covered by the codebook in the tangent space, with T_p^C covering more volume than T_m^C. The two codebooks are concatenated to form a $2^{\mathcal{B}}$ length codebook T^C. The receiver finds the optimal index c_n in T^C by comparing the chordal metric given by (1.2), of each codeword to the actual precoder $\mathbf{U}_{k,l}$ obtained from the compact SVD of the channel matrix. using (1.9). The receiver then feeds back c_n to the transmitter using $\mathcal{B}$ bits. The transmitter uses the fed back c_n and (1.10) to calculate $\tilde{\mathbf{U}}_{k,l}$,

$$c_n \leftarrow \mathrm{argmin}_{i\in 2^{\mathcal{B}}} \left(d_s\left(\mathbf{U}_{k,l}, \mathrm{retract}(\mathbf{P}_{k,l}, T^C[i])\right)\right) \tag{1.9}$$

$$\tilde{\mathbf{U}}_{k,l} = \mathrm{retract}(\mathbf{P}_{k,l}, T^C[c_n]) \tag{1.10}$$

We now describe the algorithm used to control the spread of the codebooks, as discussed in [4]. The base codebook ($\mathcal{T}^B$) consists of $2^{\mathcal{B}-1}$ matrices belonging to the local tangent space at $\mathbf{P}_{k,l}$, which represent the $2^{\mathcal{B}-1}$ quantized directions. The two codebooks, T_p^C, T_m^C, have the same set of base vectors, but different spreads g^{s_p} and g^{s_m} i.e. $T^C_{\{p/m\}} = g^{s_{\{p/m\}}}\mathrm{base}^C$ (i.e. All codewords $\in T^{\mathcal{B}}$ multiplied by $g^{s_{\{p/m\}}}$ individually). Here g is the growth factor and s_p, s_m control the spread of the two codebooks. Depending on whether $c_n \geq 2^{\mathcal{B}-1}$, i.e. whether the optimum codeword is in T_p^C or T_m^C, the scale parameter $s[k]$, which in turn controls values of s_p, s_m is updated in the following manner,

$$s_p = g^{\min(s[k-1]+1,0)}, s_m = g^{s[k-1]-1}$$

$$s[k] = \begin{cases} \min(s[k-1]+1, 0), & \text{for } c_n \in T_p^C \\ s[k-1]-1, \text{otherwise} \end{cases}$$

with $s[0] = 0$. Intuitively, the algorithm reduces/increases the spread of the codebook till the operation of reduction/increase is no longer beneficial, i.e. the optimum codeword lies in the higher/lower spread codebook instead. The scheme we use for obtaining the base codebook $\mathcal{T}^B$, however, differs slightly from the one presented in [4]. As discussed in Section 1.3, the Cayley type lifting map takes matrices residing on the Stiefel manifold and maps them to $N_T \times N_T$ skew Hermitian matrices. This allows for vector quantization of the tangent space, since a skew Hermitian matrix can be easily converted to a vector, by taking the upper triangular entries and stacking them in a vector. Vector quantization for the base codebook, $\mathcal{T}^B$ allows for isotropic $2^{\mathcal{B}-1}$ quantized directions for the tangent space local to $\mathbf{P}_{k,l}$. [4] proposed a randomly initialized $\mathcal{T}^B$ which does not guarantee isotropic $2^{\mathcal{B}-1}$ quantized directions, which can potentially hurt the performance of the system in the cases when random initialization gives directions which are close to each other. More details on codebook construction are provided in Section 1.5. This concludes the proposed predictive quantization algorithm.

The discussion thus far has not assumed a particular lifting-retraction map, and is expected to work for any appropriate lifting-retraction pair. One point to note is that, when considering (i,t) that is closest to the feedback subcarrier (k,l), we perform averaging as suggested in [21] and also used in [4] with $\tilde{\mathbf{U}}_{i,t}$ as the initial center of the averaging algorithm. Averaging over the quantization errors in the anchor point of prediction algorithm, i.e. $\tilde{\mathbf{U}}_{i,t}$, by using appropriate neighbour $\tilde{\mathbf{U}}_{j,s}$ improves the performance of the prediction algorithm. Since the averaging algorithm was suggested for the same orthographic lifting map proposed in [21], for the predictive algorithm, we use the orthographic lifting map. However, the orthographic lifting map has a higher dimension than the Cayley type maps discussed in Section 1.3. Therefore, we use the Cayley type map for the vector quantization of the tangent space.

1.4.3 Joint Time-Frequency Interpolation scheme

Once the frequency-time bin matrix has been filled according to the hopping and predictive quantization scheme proposed in Section 1.4.1, the next step at the transmitter is to fill in the non fed back boxes (k,l) in the time-frequency bins matrix. This is also done by estimating the unit step matrices, viz. $\mathcal{F}_{i,t}, \mathcal{T}_{i,t}$ at the closest fed back subcarrier (i,t) to subcarrier (k,l). To interpolate precoding matrix at (k,l), we use future nearby feed back boxes of (i,t), as shown in Fig. 1.5, since past fed back boxes' information has already been captured in the predictive quantization algorithm. Define,

$$\begin{aligned}\texttt{l\_nbrs}_{i,t}(p) &= \texttt{same\_freq\_nbrs}_{i,t}(-p) \bigcup \texttt{diff\_freq\_nbrs}_{i,t}(-p,-1),\\ \texttt{r\_nbrs}_{i,t}(p) &= \texttt{same\_freq\_nbrs}_{i,t}(-p) \bigcup \texttt{diff\_freq\_nbrs}_{i,t}(-p,1)\end{aligned}$$

as the left/right neighbors at (i,t) (marked in dark/light green, purple for $(i+3,t+1)$ in Fig. 1.5). We obtain different maps for left frequencies $\mathcal{F}^L_{i,t}, \mathcal{T}^L_{i,t}$ from $\texttt{l\_nbrs}_{i,t}(p)$, and right frequencies $\mathcal{F}^R_{i,t}, \mathcal{T}^R_{i,t}$ from $\texttt{r\_nbrs}_{i,t}(p)$, since directly obtaining $\mathcal{F}_{i,t}$ makes $\mathbf{\Delta}_{i,t}$ singular. Hence, we get the following objective functions, for obtaining $\mathcal{F}^L_{i,t}, \mathcal{T}^L_{i,t}, \mathcal{F}^R_{i,t}, \mathcal{T}^R_{i,t}$

$$\begin{aligned}\mathcal{F}^L_{i,t}, \mathcal{T}^L_{i,t} &\leftarrow \text{argmin}_{\mathsf{F}_{i,t},\mathsf{T}_{i,t}} \left(\sum_{(j,s)\in \texttt{l\_nbrs}_{i,t}(p)} \left(||(\mathsf{F}_{i,t}(j-i) + \mathsf{T}_{i,t}(s-t) - \mathbf{T}^{j,s}_{i,t})||^2_F\right)\right)\\ \mathcal{F}^R_{i,t}, \mathcal{T}^R_{i,t} &\leftarrow \text{argmin}_{\mathsf{F}_{i,t},\mathsf{T}_{i,t}} \left(\sum_{(j,s)\in \texttt{r\_nbrs}_{i,t}(p)} \left(||(\mathsf{F}_{i,t}(j-i) + \mathsf{T}_{i,t}(s-t) - \mathbf{T}^{j,s}_{i,t})||^2_F\right)\right)\end{aligned}$$

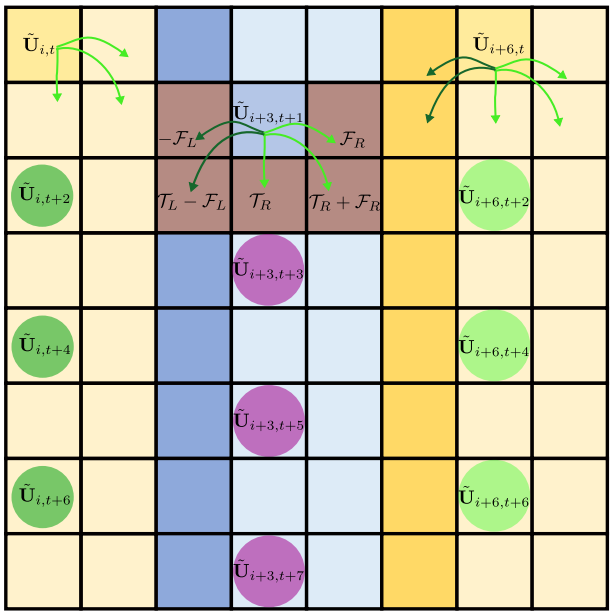

Figure 1.5: Joint interpolation strategy: Each fed back subcarrier (i,t) uses neighboring future information to estimate precoder values for $(k,l) \in \texttt{cluster}(i,t)$. The brown shaded cells form $\texttt{cluster}(i+3, t+1)$.

Hence, the interpolated estimates for non-fed back boxes (k,l) at the transmitter are given by,

$$\tilde{\mathbf{U}}_{k,l} = \begin{cases} \text{retract}(\tilde{\mathbf{U}}_{i,t}, \mathcal{F}_{i,t}^{L}(k-i) + \mathcal{T}_{i,t}^{L}(l-t)), & \text{for } k < i \\ \text{retract}(\tilde{\mathbf{U}}_{i,t}, \mathcal{F}_{i,t}^{R}(k-i) + \mathcal{T}_{i,t}^{R}(l-t)), & \text{for } k \geq i \end{cases} \tag{1.11}$$

The lifting-retraction maps used for interpolation in (1.11) are the Cayley exponential type lifting maps discussed in Section 1.3. The fed back boxes (i,t) by the receiver obtained by predictive quantization act as centers ($\tilde{\mathbf{U}}_{i,t}$ in (1.11)) to obtain the interpolated estimate of boxes $(k,l) \in \texttt{cluster}(i,t)$, which is defined as

$$\texttt{cluster}(i,t) = \begin{cases} \left\{(i-\delta_f+p, t+q) | p \in \{0,1,\ldots 2\delta_f\}, q \in \{0,1\}\right\} \setminus (i,t), & \text{for } i \neq \{0, N-1\} \\ \left\{(i+p, t+q) | p \in \{0,1,\ldots \delta_f\}, q \in \{0,1\}\right\} \setminus (i,t), & \text{for } i = 0 \\ \left\{(i-\delta_f+p, t+q) | p \in \{0,1,\ldots \delta_f\}, q \in \{0,1\}\right\} \setminus (i,t), & \text{for } i = N-1 \end{cases}$$

The joint time-frequency interpolation method is visually illustrated in Fig. 1.5. Having described the strategies used by the receiver to quantize and feed back precoding matrices, and at the transmitter to estimate the precoders at the non fed back bins of the time-frequency bins matrix, we now explain the strategy used by the receiver to quantize and the transmitter to interpolate the singular values arising from SVD. For optimal power allocation via waterfilling, the singular values should also be fed back to the transmitter. We quantize these using vector quantization and feed them back on regularly spaced subcarrier frequency indices, such as $0, 33, (33{\times}2), \ldots, (33{\times}31 = 1023)$ for 1024 subcarriers. Predictive quantization is not performed for the singular values. At the receiver, these are interpolated at the unknown subcarriers using linear interpolation,

$$\sigma_i = \left(\sigma_{\text{prev(i)}}(\text{next}(i) - i) + \sigma_{\text{next(i)}}(i - \text{prev}(i))\right) / (\text{next}(i) - \text{prev}(i))$$

where $\text{next}(i), \text{prev}(i)$ indicate the previous/next fed back point corresponding to non fed back point i, σ_j denotes the singular values corresponding to subcarrier j.

1.5 Simulation Results

The algorithms were simulated using the IT++ library through the Python wrapper pyitpp [22]. Channels were generated using Jake's model for both ITU Vehicular-A and ITU Pedestrian-A profiles, mentioned as appropriate in the following section. The simulations have been performed for $N_T = 4$ and $N_R = 2$.

SVD of a matrix is inherently not unique, and hence the computation algorithms used to perform SVD of $\mathbf{H}_{i,t}$ to obtain $\mathbf{U}_{i,t}$ as explained in Section 1.2 may not provide a continuous sequence of $\mathbf{U}_{i,t}$ matrices. Hence, it is required to correct for abrupt changes in $\mathbf{U}_{i,t}$, while simulating the algorithm, which was also performed in [4]. We have corrected for abrupt changes in $\mathbf{U}_{i,t}$ by forcing the first row of the $\mathbf{U}_{i,t}$ (viz. the left matrix obtained from SVD of $\mathbf{H}_{i,t}$, (1.1)) to have positive real numbers. This is achieved via multiplying $\mathbf{U}_{i,t}$ by diagonal matrix corresponding to conjugate angle exponentials of the complex numbers in the first row of $\mathbf{U}_{i,t}$, which ensures a continuous sequence of $\mathbf{U}_{i,t}$ obtained via SVD of $\mathbf{H}_{i,t}$.

1.5.1 Proposed Interpolation on $St(N_T, N_R)$

We consider an OFDM system with $N = 1024$ subcarriers with ITU Vehicular-A channel model for the simulation of the proposed interpolation on $St(N_T, N_R)$ and it's comparison with unitary group geodesic. The receiver feeds back the quantized precoder $\tilde{\mathbf{U}}_{i,t}$ and $\tilde{\mathcal{U}}_{i,t}$ for 32 equally spaced feedback points at indices $33k, k = 0, 1, 2 \ldots 31$. The transmitter interpolates over 4×2 $\tilde{\mathbf{U}}_{i,t}$ matrices via (1.4) and over 4×4 $\tilde{\mathcal{U}}_{i,t}$ matrices via (1.3) for precoder estimation at non-fed back subcarriers.

Codebook Generation

A 6 bit codebook for both 4×2 and 4×4 matrices is constructed using the Lloyd codebook algorithm [18]. This is done by generating 10,000 such $\mathbf{U}_{i,t}$'s and $\mathcal{U}_{i,t}$'s. We, therefore, use $32 \times 6 = 192$ bits per OFDM frame for precoder feedback for both the cases.

Results

The results in Fig. 1.6 indicate the BER performance (uncoded QPSK, MMSE equalization, 1000 symbols per subcarrier) and were obtained by averaging over 100 independent simulation runs. We observe approximately 3 dB gain at 10^{-3} BER when using the Cayley Exp. map (1.4) instead of the unitary group geodesic scheme (1.3) for interpolation. Note that, when interpolation is done over the ideal unquantized precoders (i.e. over $\mathbf{U}_{i,t}$, $\mathcal{U}_{i,t}$, instead of $\tilde{\mathbf{U}}_{i,t}$, $\tilde{\mathcal{U}}_{i,t}$), we do not observe performance benefits.

This ascertains the fact that reduction in BER is achieved since we do not quantize redundant information when interpolating directly on $\mathrm{St}(N_T, N_R)$, instead of the unitary group. $\mathrm{St}(N_T, N_R)$ is a $2N_TN_R - N_R^2$ dimensional manifold, whereas $N_T \times N_T$ unitary matrices form N_T^2 dimensional manifold. By quantizing on the unitary manifold for the purpose of using the unitary group geodesic to interpolate, we actually pay a dimensional penalty of $(N_T - N_R)^2$ while quantizing. In the chosen 4×2 MIMO configuration, by projecting matrices in $\mathrm{St}(4, 2)$ to/fro 4×4 unitary matrix and then interpolating via unitary group

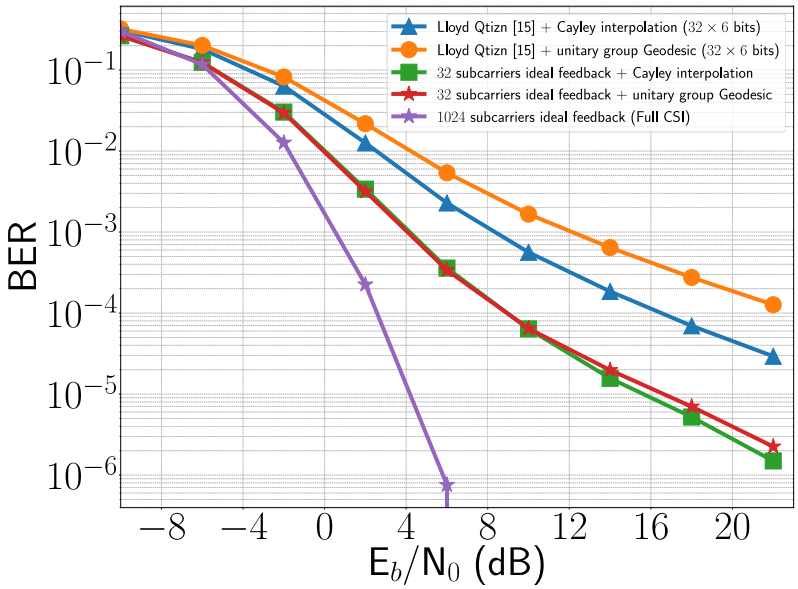

Figure 1.6: BER observed in a 4×2 MIMO system when using unitary group Geodesic interpolation [3] and Cayley Exponential interpolation as discussed in Section 1.3. The channel had the ITU Vehicular-A profile, and OFDM with 1024 subcarriers was used.

geodesic, we pay a dimensional penalty of 4. By interpolating directly over the Stiefel manifold, we avoid this dimensional penalty and hence encode more information with lesser quantization error using the same number of bits. However, in MIMO channels where $N_R \approx N_T$, the expected gain would reduce, since the dimensional penalty reduces.

When the singular values are quantized and fed back to enable waterfilling, we observe improvements in achievable rate as well. A 2 bit codebook obtained via k-means clustering of about 1000 independent sample singular values was used to feed back quantized singular values for waterfilling. By allocating 2 bits at each fed back subcarrier for the singular values, we observe a 14% improvement in achievable rate at 0 dB SNR. We see in Fig. 1.7 that the 14% improvement is not an "average" improvement, and that the proposed scheme is better than geodesic unequivocally at each subcarrier index by approximately 14%. In conclusion to this subsection, we empirically show that interpolating with the Cayley exponential map provides performance benefit over interpolating witht the unitary group geodesic.

1.5.2 Predictive Quantization and joint time-frequency based interpolation scheme

We have simulated our proposed scheme for both ITU Vehicular-A and Pedestrian-A channel models. For the Vehicular channel model, number of subcarriers N were chosen to be 1024 and for Pedestrian channel model, we chose N to be 64. We consider the hopping pattern of feedback indices (shown in Fig. 1.3), i.e. $\delta_f = 16$ (4), with $D_f = 33$ (9) when N is 1024 (64) respectively. To compare this with the time based predictive quantization and frequency interpolation scheme as in Fig. 1.2, we feed back indices of the form $33k$ ($9k$) ($N = 1024$ (64)). For interpolation in the time based approach (Fig. 1.2), we utilize the Cayley Exp. map. The simulations for the algorithm were done for a

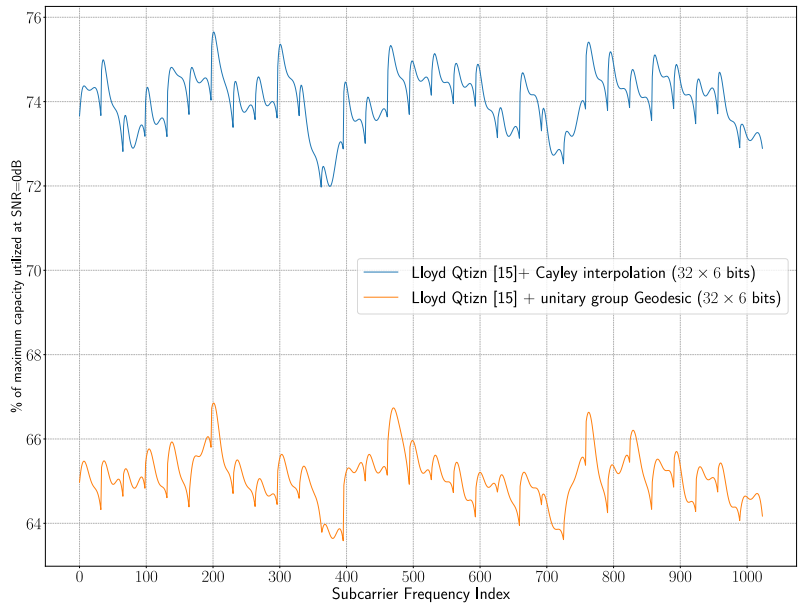

Figure 1.7: The achievable rate for a 4×2 MIMO system when using unitary group Geodesic interpolation [3] and Cayley Exponential interpolation as discussed in Section 1.3. The y-axis denotes the average instantantaneous achievable rate as a percentage of the maximum achievable rate possible given full CSI at the transmitter. Other assumptions are similar to those in Fig. 1.6.

normalized Doppler $f_d T_s = 3.5 \times 10^{-4}$, until otherwise mentioned.

Codebook generation

Since both the time based and hopping based predictive quantization methods predict based on past fed back information, we need to intitialize the system via an independent codebook based quantization [18] . We initialize the system with the 6 bit Lloyd codebook for $\mathrm{St}(4,2)$ obtained in Section 1.5.1. Once sufficient past values of $\tilde{\mathbf{U}}_{i,t}$ have been quantized and fed back in advance, the algorithms can be used to start improving upon the quantization chordal error by exploiting the correlations available. An additional 2 bit k-means codebook was used to feed back quantized singular values for waterfilling.

To obtain the base codebook, $\mathcal{T}^B$ for $T_{\mathbf{P}_{k,l}}\mathrm{St}(N_T, N_R)$, we consider 10,000 independent channel evolutions. We utilize evolution of the channel over 10 OFDM frames' duration to obtain a reliable prediction from both methods, for each fed back subcarrier. We collect the vectors representing the skew Hermitian tangents, obtained by $\mathrm{lift}_{\mathbf{P}_{k,l}}(\mathbf{U}_{k,l})$, for vector quantization (recall that Cayley Exp. map has skew Hermitian matrices as images (Section 1.3), which form a vector space). This is done to get 10,000 independent predictions for each subcarrier that give the same number of independent vectors per subcarrier in the collection. We then apply k-means ($k = 64$) algorithm over the collection obtained by stacking 10,000 vectors obtained per subcarrier, to get a 6 bit base codebook, $\mathcal{T}^B$ for $T_{\mathbf{P}_{k,l}}\mathrm{St}(N_T, N_R)$, for both the hopping based and time based predictive quantization schemes. Since k-means is applied over the stacked collection of vectors for each subcarrier, the codebook obtained is independent of choice of subcarrier. The main motive of performing this step is to ensure codewords representing isotropic directions in the tangent space. Hence we transmit $(32 \times 6 = 192)$ and $(8 \times 6 = 48)$ bits per frame when $N = 1024$ and 64 respectively for time based predictive quantization scheme. For

hopping predictive quantization scheme, the feedback is ($31.5\times6 = 189$) and ($7.5\times6 = 45$) bits per frame when $N = 1024$ and 64, since the feedback alternates between total $32, 31$ and $8, 7$ subcarriers fed back, between two frames. These feedback bits indicate the optimum tangent which the transmitter selects to refine the estimated precoder predictions for appropriate fed back subcarriers.

Estimate chordal metric, $d[t]$ results

From Fig. 1.8 we observe that with time, $d[t]$ for the hopping predictive quantization scheme becomes much lower than that of the time based approach. We observed that after a certain time instant, the chordal metric on the Stiefel Manifold bumps up, which was observed even in [4]. Hence, we propose a scheme in which the receiver resets the prediction algorithm and re-initializes with the 6 bit Lloyd codebook obtained for $\mathrm{St}(4, 2)$ when such a detrimental situation is observed. Note that, even for initialization, we communicate 192 (or 189) and 48 (or 45) bits per frame only, depending whether N is 1024 (or 64, respectively). This allows the algorithm to reset upon facing unpredictable heavy interference, since we do not assume a very heavy feedback requirement for initialization.

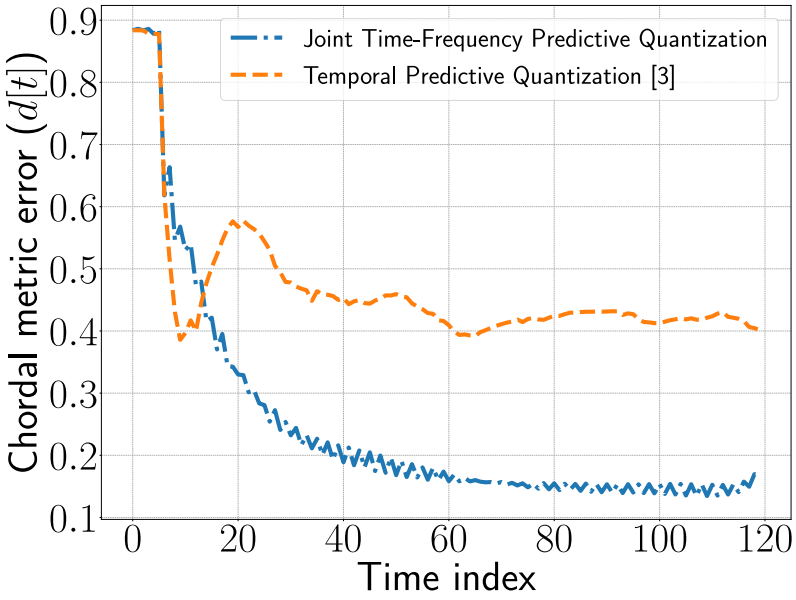

Figure 1.8: Chordal metric error ($d[t]$) vs. time for a channel realization, Vehicular channel model, 1024 subcarriers. Here, "Joint Time-Frequency Predictive Quantization" refers to the situation where the fed back points are alternated, as shown in Fig. 1.3 and interpolation performed via method discussed in Section 1.4.3. The "Temporal Predictive Quantization [4]" strategy uses the predictive quantization method in [4], with feedback points as shown in Fig. 1.2, and interpolation performed via Cayley exponential lifting map as discussed in Section 1.3.

Results for hopping scenario

Figs. 1.9a, 1.9b, shows BER performance (uncoded QPSK, MMSE equalization, 1000 symbols per subcarrier), averaged over 10 independent channel evolutions, for Vehicular, $N = 1024$ and Pedestrian, $N = 64$ respectively. In each evolution, the algorithm was run till a sudden jump in quantization error was observed (as in [4]) by the receiver. Upon encountering the jump, the receiver resets the algorithm by feeding back fresh estimates

using the independent 6 bit codebook. The jump occurs roughly after around 100 channel evolutions, and hence the necesarry feedback of 1 bit required to communicate this drastic event is minimal amortized over time.

For the Vehicular channel model, by performing predictive quantization on our hopping strategy, and doing joint time-frequency interpolation, we have matched the *ideal* 32 subcarrier feedback BER performance. The *ideal* 32 subcarrier feedback corresponds to the case in which the transmitter is assumed to know the ideal unquantized precoding matrices for 32 equally spaced subcarriers ($33k$) in each OFDM frame and interpolates over frequency by Cayley interpolation (1.4) to find precoders at non fed back subcarriers, labeled "32 subcarriers ideal feedback + Cayley interpolation" in Fig. 1.9a. The 63 subcarrier ideal feedback BER curve, labeled "63 subcarriers ideal feedback + Cayley interpolation", serves as a lower bound on the achievable BER performance for our hopping strategy. This scenario indicates that the transmitter has knowledge of ideal unquantized precoders at 32 equally spaced indices along with 31 middle indices of the regular intervals between them, in each OFDM frame, and performs interpolation as before. Hence, matching that curve would mean that we have exploited the temporal and frequency correlations perfectly, which expains why the BER of our scheme is lower bounded by this scenario. We also observe a ~2 dB gain at 10^{-4} BER, ~ 5 dB gain at 10^{-5} BER, when compared to the time based approach. One potential reason for improvements in the BER curve can be cited to the chordal metric chosen. Although the chosen metric is not a distance metric on the Stiefel manifold, it is a distance metric on the perumtation invairant flag manifold, onto which the optimal precoders for MMSE receiver reside [6]. Although we work with Stiefel manifold (which has higher dimensions than the flag manifold), we minimize the distance metric of the flag manifold, and hence we obtain such substantial improvement in the BER curve.

For the Pedestrian channel model, by performing predictive quantization via both the approaches, labeled "Indep. time-freq, [4] + Cayley interpolation (8×6 bits)", "Joint time-freq pred. qt. & interpolation (7.5×6 bits)" in Fig. 1.9b, we get huge improvements over the non-predictive independent quantization case, labeled "Cayley Exp. map (8×6 bits)". Observe that doubling the number of subcarriers fed back in the ideal cases does not offer much improvement, labeled "8/15 subcarriers ideal feedback + Cayley interpolation". This can be explained by the fact that the Pedestrian channel is strongly correlated along frequency, and thus doubling the number of subcarriers fed back does not add much to the information content. Therefore, the time domain information is more valuable in the Pedestrian channel model, and this explains why, both the predictive quantization schemes are able to improve the BER performance significantly. Even though the time domain information is more valuable, our proposed scheme, which combines both time and frequency information, still improves upon the existing approach by around 4 dB at 10^{-4} BER. However, we are not able to match the ideal performance curves, more particularly at higher SNRs, as was the case in Vehicular channel models. This can be explained due to occurrence of the error floors observed in the quantized curves at about 10^{-6} BER.

We obtain the achievable rates in Figs. 1.9c, 1.9d by averaging similarly, and the singular values are sent and interpolated as described in Section 1.5.1. The results obtained are similar for both the channel models (i.e. Vehicular and Pedestrian) considered. When

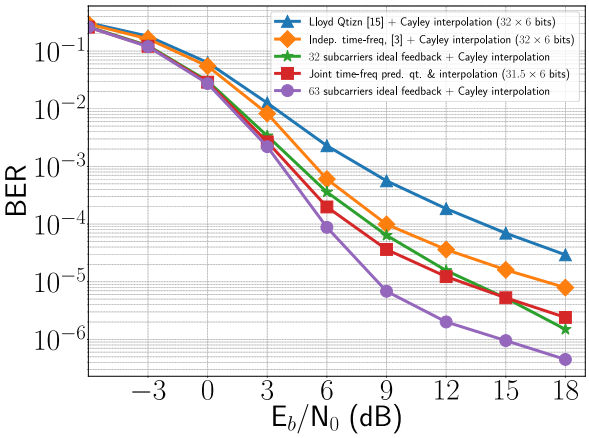

(a) BER results, Vehicular channel model

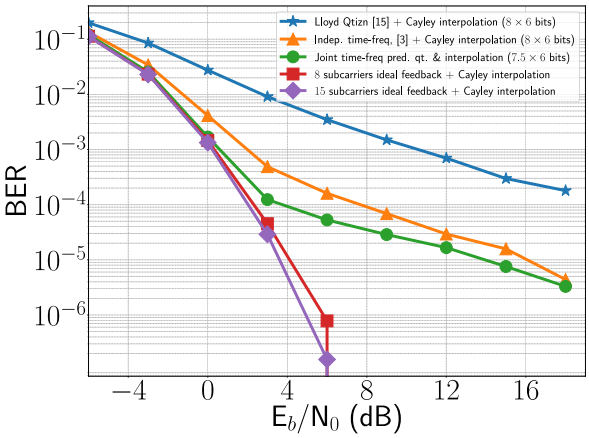

(b) BER results, Pedestrian channel model

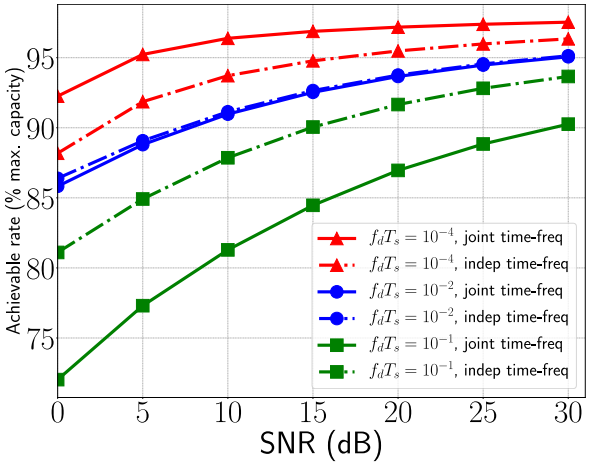

(c) Achievable rate results, Vehicular channel model

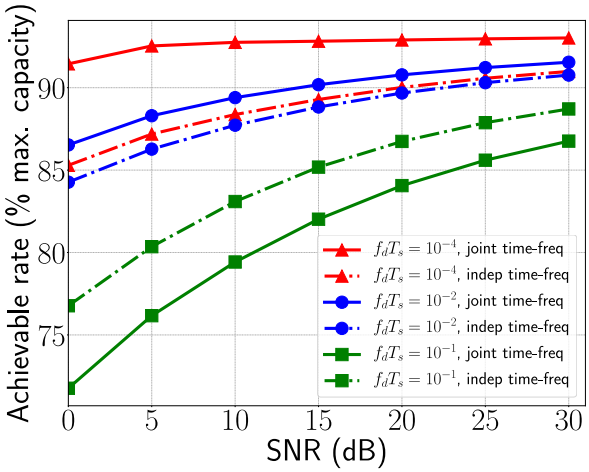

(d) Achievable rate results, Pedestrian channel model

Figure 1.9: Simulation Results for the proposed predictive quantization and joint time-frequency based interpolation scheme: Here, the Joint time-frequency based scheme refers to the situation where the fed back points are alternated, as shown in Fig. 1.3 and interpolation is performed using the method discussed in Section 1.4.3. The Independent time-frequency based scheme uses the temporal predictive quantization [4], with feedback points as shown in Fig. 1.2, and interpolation performed via Cayley exponential lifting map as discussed in Section 1.3. The y-axis for Fig. (c), (d) denotes the average instantantaneous achievable rate as a percentage of the maximum achievable rate possible given full CSI at the transmitter.

the channel varies faster, the time-based prediction tracks the channel more efficiently due to higher temporal information. For slower channels, utilizing the frequency correlation is more valuable, since the temporal variation is less significant. The crossover is at about $f_d T_s = 10^{-2}$ for both the channel models considered, which is generally a fast varying channel; we expect the hopping approach to be better in most realistic mobility scenarios.

Observe that the achievable rates at 0 dB SNR by both our proposed joint time-frequency predictive quantization scheme (Fig. 1.3, 1.5) and the independent time-frequency scheme (Fig. 1.2, [4]+[19]) comes to be $\approx 90\%$. This is significantly higher than the rate obtained via independent quantization and Cayley interpolation ($\approx 70\%$, Fig. 1.7) and illustrates the huge benefits which both the predictive quantization schemes offer over the independent quantization schemes.

1.6 Conclusions

In this paper, we have proposed a new method for interpolating precoder matrices on the Stiefel manifold for wireless MIMO systems, and empirically showed that it offers a better performance than traditional geodesic interpolation. We then proposed a hopping strategy for the location of fed back subcarriers, coupled with a predictive quantization scheme and a joint time-frequency interpolation technique to utilize the time and frequency correlations optimally. The proposed predictive quantization scheme improves quantization performance in subsequent OFDM frames and brings the BER and achievable rates close to that obtained using theoretical unquantized precoders. When compared to past approaches that utilize the same amount of feedback, our approach allows the E_b/N_0 requirement for a the BER to be reduced by $\sim$5 dB. Simultaneously, the achievable rate is also significantly boosted due to the reduced errors in precoder quantization and interpolation. Future work would involve a study with various antenna configurations and generalizing the results to the multiuser-MIMO scenario. Another interesting line of future work is to generalise the proposed algorithm to the permutation invariant flag manifold, which can potentially bring about even more improvements in the BER results, by avoiding the dimensional penalty we pay by operating on the higher dimensional Stiefel manifold.

1.7 Appendix

1.7.1 The Cayley Exponential Lifting and Retraction Pairs

Given $\mathbf{X}, \mathbf{Y} \in St(N_t, N_r)$, [19] defines the lifting map $\mathrm{Exp}_{\mathbf{X}}^{-1}(\mathbf{Y}) : St(N_t, N_r) \to T_{\mathbf{X}} St(N_t, N_r)$ by

$$\mathrm{Exp}_{\mathbf{X}}^{-1}(\mathbf{Y}) = \begin{bmatrix} \mathbf{C} & -\mathbf{B}^H \\ \mathbf{B} & \underline{0} \end{bmatrix}$$

where $\mathbf{C} = 2(\mathbf{X}_u^H + \mathbf{Y}_u^H)^{-1}\mathtt{sk}(\mathbf{Y}_u^H\mathbf{X}_u + \mathbf{X}_l^H\mathbf{Y}_l)(\mathbf{X}_u + \mathbf{Y}_u)^{-1}$ is a $N_r \times N_r$ skew hermitian matrix and $\mathbf{B} = (\mathbf{Y}_l - \mathbf{X}_l)(\mathbf{X}_u + \mathbf{Y}_u)^{-1}$ is a $(N_t - N_r) \times N_r$ matrix where, $\mathbf{X} = [\mathbf{X}_u, \mathbf{X}_l]^H$, $\mathbf{Y} = [\mathbf{Y}_u, \mathbf{Y}_l]^H$, with $\mathbf{X}_u, \mathbf{Y}_u \in \mathbb{C}^{N_r \times N_r}$ and $\mathbf{X}_l, \mathbf{Y}_l \in \mathbb{C}^{N_r \times (N_t - N_r)}$, provided that $\mathbf{X}_u + \mathbf{Y}_u$ is nonsingular, $\mathtt{sk}(\mathbf{M}) = \frac{1}{2}(\mathbf{M}^H - \mathbf{M})$. Note that $\mathrm{Exp}_{\mathbf{X}}^{-1}(\mathbf{Y})$ maps matrices residing in the Stiefel manifold to a $N_t \times N_t$ skew Hermitian matrices.

The corresponding retraction map $\text{Exp}_{\mathbf{X}}(\mathbf{T}) : T_{\mathbf{X}}St(N_t, N_r) \rightarrow St(N_t, N_r)$, with $\mathbf{X} \in St(N_t, N_r)$, $\mathbf{T} \in T_X St(N_t, N_r)$ is defined as $\text{Exp}_{\mathbf{X}}(\mathbf{T}) = \texttt{Cay}(\mathbf{T})\mathbf{X}$, where $\texttt{Cay}(\mathbf{T}) = (\mathbf{I}_{N_t} + \mathbf{T})(\mathbf{I}_{N_t} - \mathbf{T})^{-1}$ is the Cayley conformal map. Hence the unique geodesic from $\mathbf{X} \in St(N_t, N_r)$ to $\mathbf{Y} \in St(N_t, N_r)$, denoted by $\Gamma_{\mathbf{X}}^{\mathbf{Y}}(t) = \text{Exp}_{\mathbf{X}}(t\text{Exp}_{\mathbf{X}}^{-1}(\mathbf{Y}))$.

Let $\tilde{\mathbf{U}}_{i_1,t}, \tilde{\mathbf{U}}_{i_2,t} \in St(N_t, N_r)$ be the quantized precoding matrices corresponding to the i_1, i_2 subcarriers at the $t-$th time index. Then, the interpolated $\tilde{U}_{i,t}$ with $i_1 < i < i_2$ is given by,

$$\tilde{\mathbf{U}}_{i,t} = \Gamma_{\tilde{\mathbf{U}}_{i_1,t}}^{\tilde{\mathbf{U}}_{i_2,t}}\left(\frac{i-i_1}{i_2-i_1}\right) = \text{Exp}_{\tilde{\mathbf{U}}_{i_1,t}}\left(\frac{i-i_1}{i_2-i_1}\text{Exp}_{\tilde{\mathbf{U}}_{i_1,t}}^{-1}(\tilde{\mathbf{U}}_{i_2,t})\right)$$

1.7.2 Detailed steps to derive $\Delta_{i,t}$

Recall that, $\mathcal{T}_{i,t}, \mathcal{F}_{i,t}$ are matrices such that $\mathbf{T}_{i,t}^{j,s} \approx \mathcal{F}_{i,t}\Delta f + \mathcal{T}_{i,t}\Delta t$, where $\Delta f, \Delta t \in \mathbb{R}$ are small steps in the time and frequency axes respectively. We have $\Delta f = j - i$ and $\Delta t = s - t$, i.e. the signed frequency/time separation between boxes (j,t) and (i,t). With the neigbour precoders for past p samples ($\texttt{nbrs}_{i,t}(p)$) defined in (1.5), we get the following optimization framework to estimate $\mathcal{T}_{i,t}, \mathcal{F}_{i,t}$,

$$\mathcal{F}_{i,t}, \mathcal{T}_{i,t} \leftarrow \text{argmin}_{\mathsf{F}_{i,t}, \mathsf{T}_{i,t}} \sum_{(j,s)\in\texttt{nbrs}_{i,t}(p)} ||(\mathsf{F}_{i,t}(j-i) + \mathsf{T}_{i,t}(s-t) - \mathbf{T}_{i,t}^{j,s})||_F^2 \tag{1.12}$$

Now, define objective function $\mathcal{O}(\mathsf{T}_{i,t}, \mathsf{F}_{i,t}) = \sum_{(j,s)\in\texttt{nbrs}_{i,t}(p)} ||(\mathsf{F}_{i,t}(j-i)+\mathsf{T}_{i,t}(s-t)-\mathbf{T}_{i,t}^{j,s})||_F^2$. We use the identities $\frac{\partial}{\partial X}(\text{Tr}(\mathbf{AXB})) = \mathbf{A}^H\mathbf{B}^H$ and $\frac{\partial}{\partial \mathbf{X}}\left(\text{Tr}(\mathbf{AX}^H\mathbf{B})\right) = \mathbf{BA}$, where $\mathbf{A}, \mathbf{X}, \mathbf{B}$ are matrices such that the products $\mathbf{AXB}$ and $\mathbf{AX}^H\mathbf{B}$ exist. Also, recall $|\mathbf{M}|_F = \text{Tr}(\mathbf{MM}^H)$ for any matrix $\mathbf{M}$. For the sake of brevity, we write $\sum_{(j,s)\in\texttt{nbrs}_{i,t}(p)}$ as $\sum_{(j,s)}$ in the subsequent discussion. Taking the partial derivative of $\mathcal{O}(\mathsf{T}_{i,t}, \mathsf{F}_{i,t})$ with respect to $\mathsf{T}_{i,t}, \mathsf{F}_{i,t}$ we get the following equations,

$$\frac{\partial}{\partial \mathsf{F}_{i,t}}\mathcal{O}(\mathsf{T}_{i,t}, \mathsf{F}_{i,t}) = \sum_{(j,s)}\left((j-i)^2\mathsf{F}_{i,t} + (j-i)(s-t)\mathsf{T}_{i,t} - (j-i)\mathbf{T}_{i,t}^{j,s}\right)$$

$$\frac{\partial}{\partial \mathsf{T}_{i,t}}\mathcal{O}(\mathsf{T}_{i,t}, \mathsf{F}_{i,t}) = \sum_{(j,s)}\left((j-i)(s-t)\mathsf{F}_{i,t} + (s-t)^2\mathsf{T}_{i,t} - (s-t)\mathbf{T}_{i,t}^{j,s}\right)$$

Setting $\frac{\partial}{\partial \mathsf{T}_{i,t}}\mathcal{O}(\mathsf{T}_{i,t}, \mathsf{F}_{i,t})$, $\frac{\partial}{\partial \mathsf{F}_{i,t}}\mathcal{O}(\mathsf{T}_{i,t}, \mathsf{F}_{i,t})$ to null matrix gives us the following linear equation for estimation of the optimum $\mathcal{F}_{i,t}, \mathcal{T}_{i,t}$ (Observe that $\mathsf{T}_{i,t}, \mathsf{F}_{i,t}$ will come out of the summation since they do not depend on j, s):

$$\begin{bmatrix}\mathcal{F}_{i,t} \\ \mathcal{T}_{i,t}\end{bmatrix} = \mathbf{\Delta}_{i,t}^{-1}\begin{bmatrix}\Sigma_{j,s}(j-i)\mathbf{T}_{i,t}^{j,s} \\ \Sigma_{j,s}(s-t)\mathbf{T}_{i,t}^{j,s}\end{bmatrix}$$

$$\mathbf{\Delta}_{i,t} = \begin{bmatrix}\Sigma_{j,s}(j-i)^2 & \Sigma_{j,s}(j-i)(s-t) \\ \Sigma_{j,s}(j-i)(s-t) & \Sigma_{j,s}(s-t)^2\end{bmatrix}$$

This completes the detailed proof of $\Delta_{i,t}$

Chapter 2

Predictive Quantization for MIMO-OFDM SVD Precoders using Reservoir Computing Framework*

Chapter Abstract

Precoding matrices obtained from SVD of the MIMO channel matrix (which is estimated at the receiver) can be utilized at the transmitter for optimum power allocation and lower BER transmissions. A key step enabling this improved performance is the feedback of these precoders to the transmitter from the receiver. Since the bit budget for such Channel State Information (CSI) feedback is limited, these precoders need to be quantized effectively using just a few bits. For a $N_T \times N_R$ MIMO system ($N_{\{T/R\}}$: Number of Transmit/Receive Antennas), this amounts to quantizing a $N_T \times N_R$ complex-valued matrix. This task is aided by the presence of an underlying manifold structure and temporal/frequency correlations in the precoders. Predictive quantization methods exploit the available correlations in the previously estimated precoders to predict new precoders, and then quantize just the additional information required to obtain the actual precoder from the predicted value, yielding a refined estimate. In this work, we introduce a reservoir computing framework for predictive quantization by exploiting temporal correlations. Past methods have primarily exploited the nonlinear geometry of the underlying manifold structure for precoder prediction. Here, this non-linear relationship is captured using the dynamical reservoir state as part of the online training process of the reservoir. Simulations reveal that this approach produces reduced quantization error, which results in lower BER as well as improved achievable rates when compared to earlier work.

*This work has been submitted in **IEEE Globecom 2019**

2.1 Introduction

In MIMO wireless systems, precoding matrices are used for transformation of an N_S-dimensional ($N_S \leq \min(N_T, N_R)$) information vector onto an N_T-dimensional transmit vector that corresponds to the signal emanating from the N_T antennas of the transmitter. The precoding matrix used to achieve the channel capacity using optimal power allocation is obtained via the SVD of the MIMO channel matrix [2]. The MIMO channel matrix is estimated at the receiver, and the transmitter has no a-priori knowledge of the same. Therefore, to obtain the said benefits of SVD precoders at the transmitter, the receiver needs to quantize and feed back the precoders it obtains from the SVD of MIMO channel matrix. To respect the bit budget imposed by limited feedback CSI schemes, the quantization needs to be performed using very few bits. Given the high dimensionality of precoders (which form a $N_T \times N_R$ complex-valued matrix, viz. $2N_TN_R$ real numbers), effective quantization with just a few bits poses a significant challenge.

Past work has used two inherent properties of the precoders to enable effective quantization with just a few bits. First, the precoders are not actually $2N_TN_R$ dimensional entities, but have an underlying manifold structure that allows to work with lower dimensions, when performing operations over the manifold directly. Second, these precoders are correlated in both time and frequency. Utilizing these correlations permit the use of predictive quantization algorithms, which enable improvement of the quantization error with time. This improvement is obtained because utilizing the correlations for estimation of the new precoder, allows for quantization of just the small extra information needed on top of the past fed back precoders, as compared to the new precoder information in the entirety. Exploiting frequency correlations permits the use of interpolation algorithms, which reduce the feedback overhead in a single OFDM frame, by feeding back CSI only for certain subcarriers, and interpolating over the others. Combining the two inherent properties (viz. manifold structure and correlations), requires generalization of various well known linear algorithms for prediction, quantization and interpolation, to the manifold structure. This is done by exploiting the underlying non-linear differential geometry of the manifold. Relevant past work in this direction has been presented in [1, 3–5, 8, 10, 12, 23].

Manifold based approaches for predictive quantization have provided significant performance benefits, given that they work with the effective lower dimensions while framing the manifold operations to predict and quantize. However, these approaches are non-trivial, since they require specific operations over the non-linear manifold differential geometry. In this paper, we aim to capture the above non-linear relations using a reservoir computing based predictive quantizer to exploit the temporal correlations effectively. The proposed framework offers a simple solution to the predictive quantization problem, which brings about ease of implementation, along with improved performance, when compared to [4], which proposed a manifold based method of predictive quantization by exploiting temporal correlations as well.

Reservoir computing is a computational framework designed for sequential data processing. Its design is inspired from several frameworks of Recurrent Neural Networks [24], including Liquid State Machines [25] and Echo State Networks [26, 27]. The reservoir computing framework represents the non-linear relationships in the data via the higher dimensional dynamical reservoir state vector, which is transformed (using matrices, referred to as 'couplers') to the lower dimensional input/output vectors Reservoir computing

has been successfully used to solve problems like handwritten digit image recognition [25], climate prediction [27] and spoken digit recognition [28]. Reservoir computing frameworks have also been applied to solve problems in the domain of wireless communications [24, 26, 29]. [24] used reservoir computing framework to harness channel non-linearities for improved channel equalization. [26, 29] utilized the framework for OFDM symbol detection while accounting for channel and power amplifier non-linearities. In our work, we utilize a reservoir computing framework similar to one presented in [27] to capture the underlying nonlinear relations between previously obtained quantized precoders, in order to predict the precoder at next time instant. This becomes analogous to time series prediction algorithms, for which the reservoir computing framework has been cited to work effectively [26].

2.2 System Model

We consider a point-to-point $N_T \times N_R$ MIMO-OFDM wireless system. In this discussion, we assume that $N_T > N_R$ and $N_s = N_R$. The available bandwidth is divided into N subcarriers, so that, individually for each subcarrier, the channel can be assumed to be flat fading. Consistent with notation in [1, 4], the data stream received on the i-th subcarrier, t-th time instant (or the t-th OFDM frame) is denoted by:

$$\mathbf{y}_{i,t} = \mathbf{H}_{i,t}^H \tilde{\mathbf{U}}_{i,t} \mathbf{x}_{i,t} + \mathbf{w}_{i,t} \tag{2.1}$$

Here, $\tilde{\mathbf{U}}_{i,t} \in \mathbb{C}^{N_T \times N_R}$ is the quantized estimate of precoding matrix, $\mathbf{y}_{i,t} \in \mathbb{C}^{N_R \times 1}$ is the received data stream, $\mathbf{x}_{i,t} \in \mathbb{C}^{N_T \times 1}$ denotes the transmitted signal, $\mathbf{H}_{i,t} \in \mathbb{C}^{N_T \times N_R}$ denotes the MIMO channel matrix and $\mathbf{w}_{i,t}$ denotes the i.i.d. complex Gaussian noise with $\mathbf{w}_{i,t} \sim \mathcal{N}_{\mathbb{C}}(0, N_0 \mathbf{I}_{N_R})$, N_0 being the noise variance. For this work, we assume that $\mathbf{H}_{i,t}^H$ is estimated exactly, with zero error at the receiver.

If an infinite bit budget is available for precoder quantization, the transmitter can directly use the matrices obtained from SVD of $\mathbf{H}_{i,t}^H$ as the precoder $\tilde{\mathbf{U}}_{i,t}$. That is, if $\text{SVD}(\mathbf{H}_{i,t}) = \mathbf{U}_{i,t}, \Sigma_{i,t}, \mathbf{V}_{i,t}$, then $\tilde{\mathbf{U}}_{i,t} = \mathbf{U}_{i,t}$. Notice that matrices $\mathbf{U}_{i,t}$ reside on the Stiefel manifold $\text{St}(N_T, N_R)$, since the columns of $\mathbf{U}_{i,t}$ form a set of N_R orthogonal vectors in N_T dimensions [1, 4]. Given practical limitations, only limited feedback is available from the receiver, and the objective is to estimate $\mathbf{U}_{i,t}$, via $\tilde{\mathbf{U}}_{i,t}$, using the available feedback bits. Independent quantization algorithms analogous to the Lloyd codebook algorithm have been studied for quantizing $\text{St}(N_T, N_R)$ [18]. However, this approach treats precoders that are close to each other in time/frequency as independent, since it does not exploit any temporal/spectral correlations for quantization.

Predictive quantization algorithms [1, 4] can be utilized to reduce the quantization error by utilizing the available correlations. We now discuss the basic mathematical model that is central to predictive quantization algorithms for precoding matrices. Suppose that we predict the current precoding matrix based on the past p observed precoding matrices. For this, assume that $\tilde{\mathbf{U}}_{i,t-p}, \tilde{\mathbf{U}}_{i,t-p+1}, \ldots, \tilde{\mathbf{U}}_{i,t-2}, \tilde{\mathbf{U}}_{i,t-1}$ have been fed back and available at the transmitter. By using a prediction algorithm and by exploiting time correlations among precoders at time instances $t-p, t-p+1, \ldots, t-2, t-1$, the transmitter can obtain a prediction (viz. a coarse estimate) of $\mathbf{U}_{i,t}$, given by

$\mathbf{P}_{i,t} = f_P(\tilde{\mathbf{U}}_{i,t-p}, \tilde{\mathbf{U}}_{i,t-p+1}, \ldots, \tilde{\mathbf{U}}_{i,t-2}, \tilde{\mathbf{U}}_{i,t-1})$, where $f_P : \mathrm{St}(N_T, N_R) \times \ldots \{p - \text{times}\} \ldots \times \mathrm{St}(N_T, N_R) \rightarrow \mathrm{St}(N_T, N_R)$ is a prediction function. Now, since the transmitter already possesses a coarse estimate $\mathbf{P}_{i,t}$ of $\mathbf{U}_{i,t}$, the receiver just quantizes the local space of $\mathrm{St}(N_T, N_R)$ nearby $\mathbf{P}_{i,t}$, instead of the complete $\mathrm{St}(N_T, N_R)$. The receiver feeds back this quantized information, enabling a refined estimate of $\mathbf{U}_{i,t}$, given by $\tilde{\mathbf{U}}_{i,t}$ at the transmitter. That is, the transmitter utilizes a quantization function $q_P : \mathrm{St}(N_T, N_R) \times \mathbb{N} \rightarrow \mathrm{St}(N_T, N_R)$, to obtain $\tilde{\mathbf{U}}_{i,t} \leftarrow q_P(\mathbf{P}_{i,t}, \mathrm{fb}_{i,t})$, where $\mathrm{fb}_{i,t} \in \{1, 2 \ldots 2^{\mathcal{B}}\}$ is the feedback from the receiver for precoder at i-th subcarrier and t-th time instant, considering bit budget of $\mathcal{B}$ bits. In [1, 4, 5], $\mathrm{fb}_{i,t}$ denotes the codeword index for the codebook obtained for quantizing the local tangent space at $\mathbf{P}_{i,t}$.

When using the predictive quantization scheme, the quantization is performed on a smaller subspace when compared to the entire manifold in case of independent quantization. Therefore, the quantization error is substantially lower as well. However, independent quantization algorithms are important for smart initialization (instead of a cold start) of the predictive quantization strategies. Observe that predictive quantization algorithms for SVD precoders are typically the higher dimensional analogues of well known approaches to reduce quantization error using linear prediction codes (LPCs) and Delta PCM. In both LPCs and Delta PCM, quantization error can be reduced substantially using a linear predictor and quantizing the scalar difference between the predicted and observed value (innovation). Analogous to this, for $\mathrm{St}(N_T, N_R)$, quantization error is reduced by quantizing a subspace around the predicted value that is much smaller than the entire manifold.

In our work, we propose a reservoir computing based prediction framework that predicts the new precoders by utilizing temporal correlations that are captured from past observed precoders (via f_P). We reuse the q_P algorithm from [1, 4]. However, by incorporating the q_P in the reservoir framework, f_P and q_P get coupled in the sense that f_P is optimized via online training of the reservoir by minimizing the norm difference between $\mathbf{P}_{i,t} = f_P(\cdot)$, and $\tilde{\mathbf{U}}_{i,t} = q_P(f_P(\cdot), \mathrm{fb}_{i,t})$. Previous work [1, 4] has considered f_P and q_P to be uncoupled with each other. A detailed discussion on the reservoir computing based model for f_P and q_P is presented in Section 2.3. The proposed reservoir computing scheme is evaluated against the temporal predictive quantization scheme in [4], and the simulation results are discussed in Section 2.4.

2.3 Reservoir Framework for Predictive Quantization

2.3.1 Vectorizing matrices in the Stiefel Manifold

The reservoir computing framework has inputs and outputs as real vectors, and thus, it is necessary to convert the precoding matrices to vectors. A precoding matrix $\mathbf{M} \in \mathrm{St}(N_T, N_R)$ is a $\mathbb{C}^{N_T \times N_R}$ matrix with the property $\mathbf{M}^H\mathbf{M} = \mathbf{1}_{N_R}$. For brevity, we call such a matrix $\mathbf{M}$ a 'semi-unitary' matrix. A naïve method to vectorize a $\mathbb{C}^{N_T \times N_R}$ semi-unitary matrix would be to take all its $N_T N_R$ complex numbers individually and stack them onto a $2N_T N_R$ dimensional real vector. However, a more efficient approach would be to use the $\mathbf{M}^H\mathbf{M} = \mathbf{1}_{N_R}$ property, which implies that each vector that represents the columns of $\mathbf{M}$ is orthogonal to the other columns. For the first column, we take its N_T complex numbers

and stack them onto a $2N_T$ vector. For the second column, we take only the first $N_T - 1$ complex numbers and concatenate, since the last number can be determined by utilizing orthogonality with the first column. For the third column, we take only the first $N_T - 2$ complex numbers, and so on. Therefore, we vectorize a $\mathbb{C}^{N_T \times N_R}$ semi-unitary matrix into a $2(N_T) + 2(N_T - 1) + \ldots + 2(N_T - N_R + 1) = 2N_T N_R - N_R^2 + N_R$ dimensional vector.

Observe here that we incur a dimensional penalty upon vectorizing semi-unitary matrices. $\mathrm{St}(N_T, N_R)$ is a $2N_T N_R - N_R^2$ dimensional manifold, whereas the proposed vectorization yields a $2N_T N_R - N_R^2 + N_R$ dimensional vector representation. This corresponds to an overhead of N_R dimensions, since we have not exploited the fact that each of the N_R column vectors is a unit norm vector as well. It looks as if utilizing the norm 1 property, we could just take $N_T - 1$ complex numbers when vectorizing the first column, instead of N_T. However, this would lead to non-unique representations, since there could then be infinite possible values that the lone missing complex number can take, so that the vector has unit norm. Hence, we vectorize a semi-unitary $\mathbb{C}^{N_T \times N_R}$ $\mathbf{M}$ into $2N_T N_R - N_R^2 + N_R$ dimensional vector, denoted as $\mathbf{m}$.

2.3.2 Forward Prediction f_P

The vector representation of semi-unitary matrices allows to proceed with our discussion on reservoir computing framework. Consider the reservoir computing framework depicted in Fig. 2.1

The input to the reservoir i that corresponds to subcarrier i is $\tilde{\mathbf{u}}_{i,t-1}$ (vectorized representation of $\tilde{\mathbf{U}}_{i,t-1}$), with dimensions $D_{\text{in}} = 2N_T N_R - N_R^2 + N_R$. Using a randomly initialized $D_{\text{resv}} \times D_{\text{in}}$ input coupler matrix $\mathbf{W}_i^{\text{in}}$, the D_{in} dimensional input is mapped to a $D_{\text{resv}}(>> D_{\text{in}})$ dimensional vector, where D_{resv} is the dimension of the reservoir state vector $\mathbf{r}_{i,t}$. $\mathbf{r}_{i,t}$ is initialized with D_{resv} zeros, and is updated via the following equation:

$$\mathbf{r}_{i,t} = \tanh(\mathbf{A}_i \mathbf{r}_{i,t-1} + \mathbf{W}_i^{\text{in}} \tilde{\mathbf{u}}_{i,t-1}) \tag{2.2}$$

where $\mathbf{A}_i$ is the adjacency matrix that captures the reservoir dynamics, and tanh is applied element wise. Typical choices for $\mathbf{A}_i$ have been Erdos-Renyi graphs with an upper bounded maximum eigenvalue [26, 27]. The output of the reservoir is $\mathbf{p}_{i,t}$, a vectorized representation of $\mathbf{P}_{i,t}$, which denotes the predicted precoder at i-th subcarrier, t-th time instant. Therefore, the output of the reservoir is also a D_{in} dimensional vector (viz. $D_{\text{out}} = D_{\text{in}}$). The output $\mathbf{p}_{i,t}$ is obtained using a matrix transformation of the reservoir state $\mathbf{r}_{i,t}$ with the $D_{\text{out}} \times D_{\text{rev}}$ output coupler matrix $\mathbf{W}_{i,t-1}^{\text{out}}$,

$$\mathbf{p}_{i,t} = \mathbf{W}_{i,t-1}^{\text{out}} \mathbf{r}_{i,t} \tag{2.3}$$

This completes the forward prediction to obtain $\mathbf{P}_{i,t}$ using only the past observed $\mathbf{U}_{i,t-1}$ (i.e. $p = 1$, Section 2.2). That is,

$$\mathbf{P}_{i,t} = f_P(\tilde{\mathbf{U}}_{i,t-1}) = \mathbf{W}_{i,t-1}^{\text{out}} \tanh(\mathbf{A}_i \mathbf{r}_{i,t-1} + \mathbf{W}_i^{\text{in}} \tilde{\mathbf{u}}_{i,t-1})^1 \tag{2.4}$$

However, a complete discussion of the framework involves a backward pass for reservoir training, which estimates optimum $\mathbf{W}_{i,t}^{\text{out}}$. This would follow subsequently after $q_P(\cdot)$ is described.

[1] For brevity, $\mathbf{p}_{i,t}$ and $\mathbf{P}_{i,t}$ are treated to be one and the same

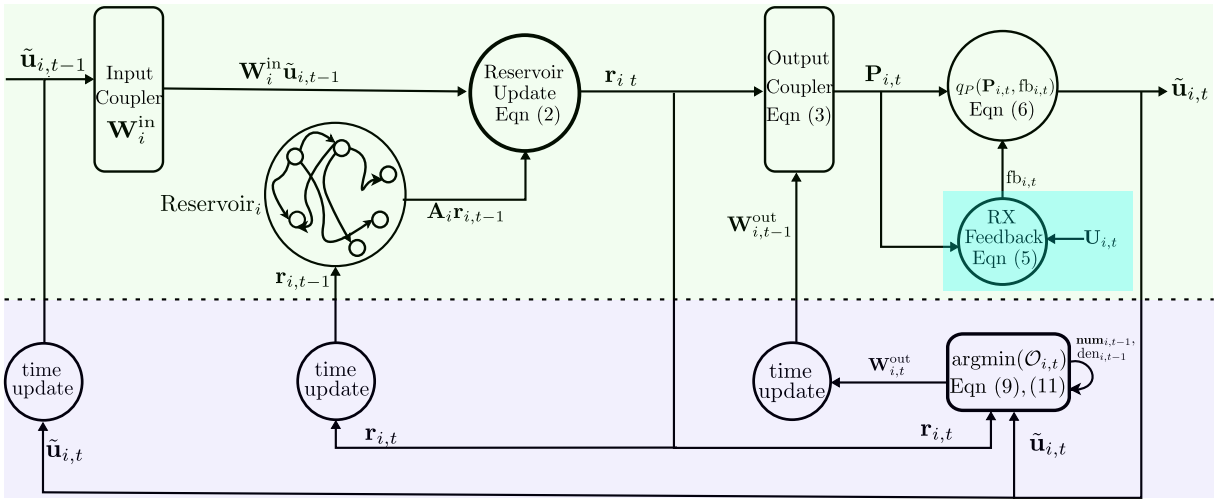

Figure 2.1: **Forward Prediction (Green)**: Both the transmitter and receiver utilize identical reservoirs and quantized precoder estimate at $t-1$ (i.e. $\tilde{\mathbf{u}}_{i,t-1}$, top left of fig.) to obtain $\mathbf{P}_{i,t}$ via (2.4). The transmitter estimates the quantized precoder at t (i.e. $\tilde{\mathbf{u}}_{i,t}$, top right of fig.) using receiver feedback $\text{fb}_{i,t}$ via q_P (2.6). **Feedback Estimation (Cyan)**: The Receiver estimates the ideal $\text{fb}_{i,t}$ using the exact precoders $\mathbf{U}_{i,t}$ via (2.5). The transmitter observes only the feedback $\text{fb}_{i,t}$ **Backward Pass (Blue)**: $\mathbf{W}_{i,t}^{\text{out}}$ is updated via (2.11) for optimizing $\mathcal{O}_{i,t}$. This is done at both transmitter and receiver to ensure identical evolution of the reservoirs

2.3.3 Quantization function q_P

We now describe the quantization function $q_P(\mathbf{P}_{i,t}, \text{fb}_{i,t})$, which is similar to the schemes used in [1, 4, 5]. Central to the quantization algorithm is the fact that tangent spaces local to a point in manifold are vector spaces. Given two points $\mathbf{X}$ and $\mathbf{Y}$ in $\text{St}(N_T, N_R)$, a lifting operation $\mathbf{T}_X^Y = \texttt{lift}(\mathbf{X}, \mathbf{Y})$, $\texttt{lift} : \text{St}(N_T, N_R) \times \text{St}(N_T, N_R) \rightarrow \mathcal{T}_X\text{St}(N_T, N_R)$ yields a tangent from X to Y, denoted as $\mathbf{T}_X^Y \in \mathcal{T}_X\text{St}(N_T, N_R)$, where $\mathcal{T}_X\text{St}(N_T, N_R)$ is the local tangent space at $\mathbf{X}$. A corresponding retraction operation $Y = \texttt{retract}(X, \mathbf{T}_X^Y)$, $\texttt{retract} : \text{St}(N_T, N_R) \times \mathcal{T}_X\text{St}(N_T, N_R) \rightarrow \text{St}(N_T, N_R)$ gives back the manifold point obtained by traversing in the tangent direction given by the second argument ($\mathbf{T}_X^Y$). In this work, the chosen lifting-retraction pairs are the Cayley exponentials, discussed in [1, 19]. The Cayley exponential lifting operation maps two points in $\text{St}(N_T, N_R)$, to a $N_T \times N_T$ skew Hermitian matrix that represents the tangent from first point to the other.

The quantization algorithm exploits the vector space property of the tangent space and quantizes the local tangent space at the predicted precoder $\mathbf{P}_{i,t}$, viz $\mathcal{T}_{\mathbf{P}_{i,t}}\text{St}(N_T, N_R)$. The codebook for $\mathcal{T}_{\mathbf{P}_{i,t}}\text{St}(N_T, N_R)$ corresponds to a collection of $\mathcal{B} - 1$ codewords that represent the different directions (tangents) in $\mathcal{T}_{\mathbf{P}_{i,t}}\text{St}(N_T, N_R)$. This codebook is subsequently referred to as the base codebook (base$^{\mathcal{C}}$) for the quantization function. The feedback from the receiver indicates the codeword corresponding to the optimum tangent in the base$^{\mathcal{C}}$, which the transmitter can choose to get closest (in terms of chordal distance metric, $d_s(\mathbf{X}, \mathbf{Y})$ for $\mathbf{X}, \mathbf{Y} \in \text{St}(N_T, N_R)$ detailed in [1, 4]) to the actual value $\mathbf{U}_{i,t}$. With the optimum direction chosen, the next step is to determine how much to move in that particular chosen direction, viz. the length of the chosen tangent direction.

For this, we adopt the strategy in [4], which controls the magnitude of tangent steps, by having two codebooks $T_p^{\mathcal{C}}, T_m^{\mathcal{C}}$ of different spreads s_p, s_m, but the same $2^{\mathcal{B}-1}$ base vectors

in the base$^{\mathcal{C}}$, i.e. $T^{\mathcal{C}}_{\{p/m\}} = s_{\{p/m\}}\text{base}^{\mathcal{C}}$ (i.e. All codewords $\in$ base$^{\mathcal{C}}$ multiplied by $s_{\{p/m\}}$ individually). The two codebooks are concatenated to form a $2^{\mathcal{B}}$ length codebook, $T^{\mathcal{C}}$. The receiver finds the optimal index $\text{fb}_{i,t} \in \{1, 2, \ldots, 2^{\mathcal{B}}\}$ in $T^{\mathcal{C}}$ by comparing the chordal distance metric (d_s), of each codeword to the actual precoder $\mathbf{U}_{i,t}$ obtained from the SVD of the channel matrix, using (2.5). The receiver then feeds back $\text{fb}_{i,t}$ to the transmitter using $\mathcal{B}$ bits. The transmitter uses the fed back $\text{fb}_{i,t}$ and (2.6) to calculate $\tilde{\mathbf{U}}_{i,t}$,

$$\text{fb}_{i,t} \leftarrow \text{argmin}_{i\in\{1,2,\ldots,2^{\mathcal{B}}\}} \left(d_s \left(\mathbf{U}_{i,t}, \text{retract}(\mathbf{P}_{i,t}, T^{\mathcal{C}}[i])\right)\right) \tag{2.5}$$

$$\tilde{\mathbf{U}}_{i,t} = q_P(\mathbf{P}_{i,t}, \text{fb}_{i,t}) = \text{retract}(\mathbf{P}_{i,t}, T^{\mathcal{C}}[\text{fb}_{i,t}]) \tag{2.6}$$

$\text{fb}_{i,t}$ is also used to update the spread of the codebooks $T^{\mathcal{C}}_p, T^{\mathcal{C}}_m$. Depending on whether $\text{fb}_{i,t} \geq 2^{\mathcal{B}-1}$, i.e. whether the optimum codeword is in $T^{\mathcal{C}}_p$ or $T^{\mathcal{C}}_m$, the scale parameter $s[k]$, which in turn controls values of s_p, s_m, is updated as,

$$s_p = g^{\min(s[k-1]+1,0)}, s_m = g^{s[k-1]-1}$$

$$s[k] = \begin{cases} \min(s[k-1]+1, 0), \text{ for } \text{fb}_{i,t} \in T^{\mathcal{C}}_p \\ s[k-1]-1, \text{otherwise} \end{cases}$$

with $s[0] = 0$. Intuitively, the algorithm reduces/increases the spread of the codebook till the reduction/increase of spread is no longer beneficial, i.e. the optimum codeword lies in the higher/lower spread codebook instead. The scheme used to obtain base$^{\mathcal{C}}$ is similar to the one presented in [1], which performs a k-means ($k = 2^{\mathcal{B}-1}$) clustering on a collection of tangents to obtain an isotropic collection of $2^{\mathcal{B}-1}$ tangent codewords. This completes the discussion on the quantization function q_P to obtain $\tilde{\mathbf{U}}_{i,t} = q_P(\mathbf{P}_{i,t}, \text{fb}_{i,t})$ from $\mathbf{P}_{i,t}, \text{fb}_{i,t}$.

2.3.4 Reservoir Training Procedure, the backward pass

Having described the technicalities of f_P, q_P, we now describe the training process for the reservoir, which couples f_P with q_P. Recall that, to obtain $\tilde{\mathbf{U}}_{i,t}$ from $\tilde{\mathbf{U}}_{i,t-1}$, we have

$$\tilde{\mathbf{U}}_{i,t} = q_P(\mathbf{P}_{i,t}, \text{fb}_{i,t}) = q_P(f_P(\tilde{\mathbf{U}}_{i,t-1}), \text{fb}_{i,t}) \tag{2.7}$$

The key idea for reservoir training is that, as the predicted matrix $\mathbf{P}_{i,t}$ (the coarse estimate) gets closer to $\tilde{\mathbf{U}}_{i,t}$ (the refined estimate), the receiver has to quantize even smaller subspaces, and can thus provide a more refined estimate from the feedback $\text{fb}_{i,t}$. Hence, we train the reservoir output coupler such that the following objective function is optimized:

$$O_{i,t} = \sum_{s=1}^{t} \frac{1}{\lambda^{t-s}} ||\mathbf{p}_{i,t} - \tilde{\mathbf{u}}_{i,t}||^2 = \sum_{s=1}^{t} \frac{1}{\lambda^{t-s}} ||\mathbf{W}^{\text{out}}_{i,t}\mathbf{r}_{i,t} - \tilde{\mathbf{u}}_{i,t}||^2 \tag{2.8}$$

Here $\lambda > 1$ is the history parameter, and $||\cdot||$ is $\mathcal{L}^2$ norm. We wish to perform the following optimization in order to find the optimum $\mathbf{W}^{\text{out}}_{i,t}$ from the available estimates till time t:

$$\mathbf{W}^{\text{out}}_{i,t} \leftarrow \text{argmin}_{\mathbf{W}^{\text{out}}_{i,t}} (O_{i,t} = \sum_{s=1}^{t} \frac{1}{\lambda^{t-s}} ||\mathbf{W}^{\text{out}}_{i,t}\mathbf{r}_{i,t} - \tilde{\mathbf{u}}_{i,t}||^2) \tag{2.9}$$

Computing the gradient $\frac{\partial O_{i,t}}{\partial \mathbf{W}_{i,t}^{\text{out}}}$ and setting it to null yields,

$$\mathbf{W}_{i,t}^{\text{out}} = \frac{\sum_{s=1}^{t} \frac{1}{\lambda^{t-s}} \texttt{outer}(\tilde{\mathbf{u}}_{i,s}, \mathbf{r}_{i,s})}{\sum_{s=1}^{t} \frac{1}{\lambda^{t-s}} ||\mathbf{r}_{i,s}||^2} \tag{2.10}$$

where $\texttt{outer}(\mathbf{x}, \mathbf{y})$ is the outer product between N_x dimensional vector $\mathbf{x}$ and N_y dimensional vector $\mathbf{y}$ to yield a $N_x \times N_y$ matrix. Let $\sum_{s=1}^{t} \frac{1}{\lambda^{t-s}} \texttt{outer}(\tilde{\mathbf{u}}_{i,s}, \mathbf{r}_{i,s})$ be $\mathbf{num}_{i,t}$ and $\sum_{s=1}^{t} \frac{1}{\lambda^{t-s}} ||\mathbf{r}_{i,s}||^2$ be $\text{den}_{i,t}$, with $\mathbf{W}_{i,t}^{\text{out}} = \frac{\mathbf{num}_{i,t}}{\text{den}_{i,t}}$. Observe that

$$\mathbf{W}_{i,t}^{\text{out}} = \frac{\frac{\mathbf{num}_{i,t-1}}{\lambda} + \texttt{outer}(\tilde{\mathbf{u}}_{i,t}, \mathbf{r}_{i,t})}{\frac{\text{den}_{i,t-1}}{\lambda} + ||\mathbf{r}_{i,t}||^2} \tag{2.11}$$

(2.11) makes training of the reservoir easy to implement with low complexity. We only need to store a matrix $\mathbf{num}_{i,t-1}$, and a number $\text{den}_{i,t-1}$. Then, using the current reservoir state $\mathbf{r}_{i,t}$ and $\tilde{\mathbf{u}}_{i,t}$ obtained from (2.2), (2.7) respectively, optimum $\mathbf{W}_{i,t}^{\text{out}}$ can be estimated. The optimum $\mathbf{W}_{i,t}^{\text{out}}$ can then be used to obtain $\tilde{\mathbf{P}}_{i,t+1}$, and so on. This completes the discussion of the proposed reservoir computing framework illustrated in Fig. 2.1.

To conclude this section, we summarize and highlight the novel aspects of the proposed framework. The first key advantage of the proposed approach over the past work [1, 4, 5] is that here the prediction function, f_P is coupled with the quantization function, q_P. Past work for predictive quantization has largely kept f_P and q_P uncoupled in the sense that, the obtained precoder is just composite function of f_P and q_P, applied to the previous p precoder estimates i.e. $q_P(f_P(\cdot))$ (Section 2.2). In the proposed framework, f_P changes with time due to the update equation of $\mathbf{W}_{i,t}^{\text{out}}$ (2.11). Recall that $\mathbf{W}_{i,t}^{\text{out}}$ update equation is obtained from optimizing (2.8), which minimizes the norm error between the prediction $\mathbf{p}_{i,t}$ (the coarse estimate) and the quantized value $\tilde{\mathbf{u}}_{i,t}$ (the refined estimate). Hence, backward pass ensures that the coarse estimate provided by f_P gets more refined with time, since optimizing $\mathbf{W}_{i,t}^{\text{out}}$ to minimize $O_{i,t}$ brings the predicted estimates $\mathbf{p}_{i,s\leq t}$ closer to the quantized estimates $\tilde{\mathbf{u}}_{i,s\leq t}$. The updated $\mathbf{W}_{i,t}^{\text{out}}$ is then used to obtain $\mathbf{P}_{i,t+1}$, which is likely to be closer to $\tilde{\mathbf{U}}_{i,t+1}$, than $\mathbf{P}_{i,t}$ was to $\tilde{\mathbf{U}}_{i,t}$, due to optimization of $O_{i,t}$. This enables q_P to quantize even smaller subspaces, since the coarse estimate itself has improved, which in turn brings about lower quantization error, and thus improved performance.
Another advantage of the proposed scheme is the ease of training of the reservoir, entailed by (2.11). Reservoir computing, thus proposes an easy to train data centric scheme, which is not typical for data centric ML based schemes. Also, by storing just one matrix $\mathbf{num}_{i,t}$ and a number $\text{den}_{i,t}$, we capture the entire history of the obtained quantized precoders, with past values weighted by λ in $O_{i,t}$ (2.8). This is a departure from previous schemes [1, 4, 5] which store the past p precoders in a p sized cyclic buffer (p also has to be pre-decided).

2.4 Simulation Results

2.4.1 Simulation setting considered

The simulations have been performed for the IEEE Pedestrian-A channel, with $N_T = 4$, $N_R = 2$. The channel matrices $\mathbf{H}_{i,t}$ are generated using Jake's model via IT++ library

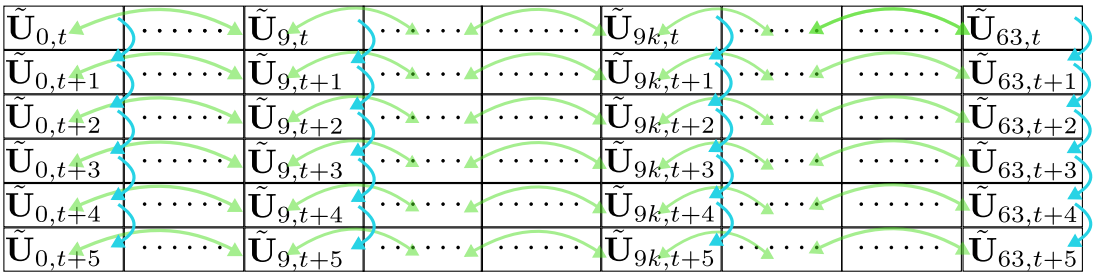

Figure 2.2: The transmitter obtains feedback for $\{9k, k \in \{0, 1, \ldots, 7\}$ subcarriers, and uses $\tilde{\mathbf{U}}_{i,t-1}$, along with f_P, q_P (2.7) to obtain $\tilde{\mathbf{U}}_{i,t}$, illustrated in the figure via cyan arrows. For each time instant, the transmitter uses the Cayley method (2.12) to interpolate $\tilde{\mathbf{U}}_{i,t}$ at $i \neq \{9k\}$ non fed back subcarriers (green arrows

through the python wrapper py-itpp [22]. We compare the results obtained by our framework with [4], which presented a manifold geometry method to exploit temporal correlations for predictive quantization. We keep $p = 4$ for the f_P presented in [4]. The quantization function q_P is kept to be same, as described in [1, 4, 5] for both the approaches. Although in both our work and [4], only temporal correlations are exploited, we compare the simulation results for the complete MIMO-OFDM setting (visually illustrated in Fig. 2) with $N = 64$ subcarriers. Channels are fed back for 8 evenly spaced subcarriers indexed from 0, viz. $\{0, 9, \ldots, 63\}$ ($\{9k, k \in \{0, 1, \ldots, 7\}\}$). Hence, the transmitter obtains only $\text{fb}_{\{9k\},t}$. For non fed back subcarriers $i \neq 9k$, $9n < i < 9(n+1)$, the Cayley method [1] is used to interpolate $\tilde{\mathbf{U}}_{i,t}$, from available estimates, $\tilde{\mathbf{U}}_{9n,t}$ and $\tilde{\mathbf{U}}_{9(n+1),t}$

$$\tilde{\mathbf{U}}_{i,t} = \text{Exp}_{\tilde{\mathbf{U}}_{9n,t}}\left((i/9 - n)\text{Exp}^{-1}_{\tilde{\mathbf{U}}_{9n,t}}\left(\tilde{\mathbf{U}}_{9(n+1),t}\right)\right) \tag{2.12}$$

For a detailed treatment on $\text{Exp}, \text{Exp}^{-1}$, refer [19].

A 6 bit codebook generated using the Lloyd codebook algorithm for the Stiefel Manifold presented in [18] is used for initial feedback ($\tilde{\mathbf{U}}_{\{9k\},0}$) and differential quantization (i.e. $\mathbf{P}_{i,t} = \tilde{\mathbf{U}}_{i,t-1}$) is used for 10 time instances to provide the initial training data for the reservoir and to overcome the initial transient response of the reservoir (also discussed in [26]). A 5 bit base codebook is used for the quantization function q_P and is generated according to the method presented in Section 2.3.3, similar to [1]. Hence, both initialization and subsequent feedback, $\text{fb}_{i,t}$ can be encoded using 6 bits (i.e. $\mathcal{B} = 6$ Section 2.2). The bit budget per OFDM frame is thus 48 bits, for total 8 equally spaced fed back subcarriers $\{9k, k \in \{0, 1, \ldots, 7\}\}$.

For predicting channels at each of the 8 fed-back subcarriers, we consider 8 separate reservoirs, each of them evolved separately, with $i \in \{9k, k \in \{0, 1, \ldots, 7\}\}$ in both the forward pass prediction and quantization (f_P, q_P) (2.7) and backward pass to update $\mathbf{W}^{\text{out}}_{i,t}$ (2.10). Unlike [1], we do not exploit frequency correlations for predictive quantization, and the 8 reservoirs for prediction of 8 fed-back subcarriers are kept independent of each other. All these 8 reservoirs are initialized with $\mathbf{A}_{i\in\{9k\}}$ being an Erdos-Renyï graph, with probability of edge connections being 0.2, $\lambda = 2$, $\mathbf{W}^{\text{out/in}}_{i\in\{9k\},0}$ initialized randomly, $D_{\text{in}} = D_{\text{out}} = 14$ (vectorized representation of 4×2 semi-unitary matrix, Section 2.3.1) and $D_{\text{resv}} = 60$.

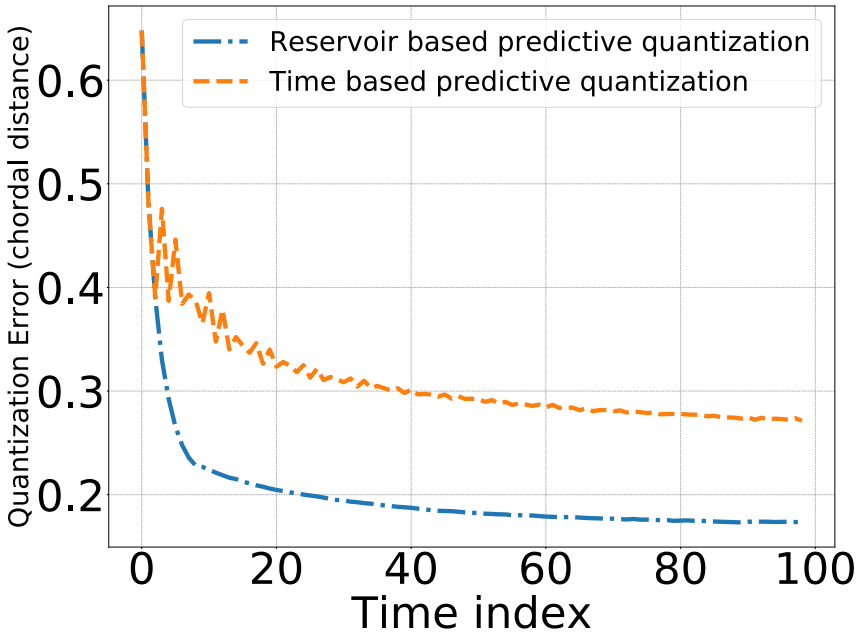

Figure 2.3: Quantization error in terms of chordal distance to the actual precoder $\mathbf{U}_{\{9k\},t}$ observed at the receiver, from the quantized estimate $\tilde{\mathbf{U}}_{\{9k\},t}$ averaged over $\{9k\}$ fed back subcarriers $\left(\text{viz. } \frac{\Sigma_{i\in 9k} d_S(\tilde{\mathbf{U}}_{i,t},\mathbf{U}_{i,t})}{8}\right)$ and 10 independent channel realizations (normalized Doppler $f_D T_s = 10^{-4}$).

2.4.2 Quantization error, BER and Achievable Rate Results

To ensure that the simulation results hold in general for the chosen IEEE Pedestrian A channel profile, we perform averaging over 10 independent channel realizations. Therefore, the quantization error, BER and achievable rate results are averaged over 1000 channel instances, with 100 channel evolutions of 10 independent channel realizations.

From Fig. 2.3 it is evident that the proposed framework is able to reduce the quantization error below what was obtained from the existing temporal correlations based predictive quantizer in [4]. In addition, the quantization error plot is much smoother as well, which can be explained from the fact that the reservoir computing approach optimizes $O_{i,t}$, that captures the long term dynamics of the channel and hence, does not face jittery variations. We simulate (uncoded QPSK) BER performance for all the 64 subcarriers' precoders obtained after interpolation ($\tilde{\mathbf{U}}_{i\neq\{9k\},t}$) and quantization ($\tilde{\mathbf{U}}_{\{9k\},t}$). Observe from Fig. 2.4 that reservoir computing framework is able to achieve substantial improvements in $\mathrm{E_bN_0}$ levels at BER $\leq 10^{-4}$. Particularly, for BER $= 10^{-5}$ we observe around 5 dB improvement.

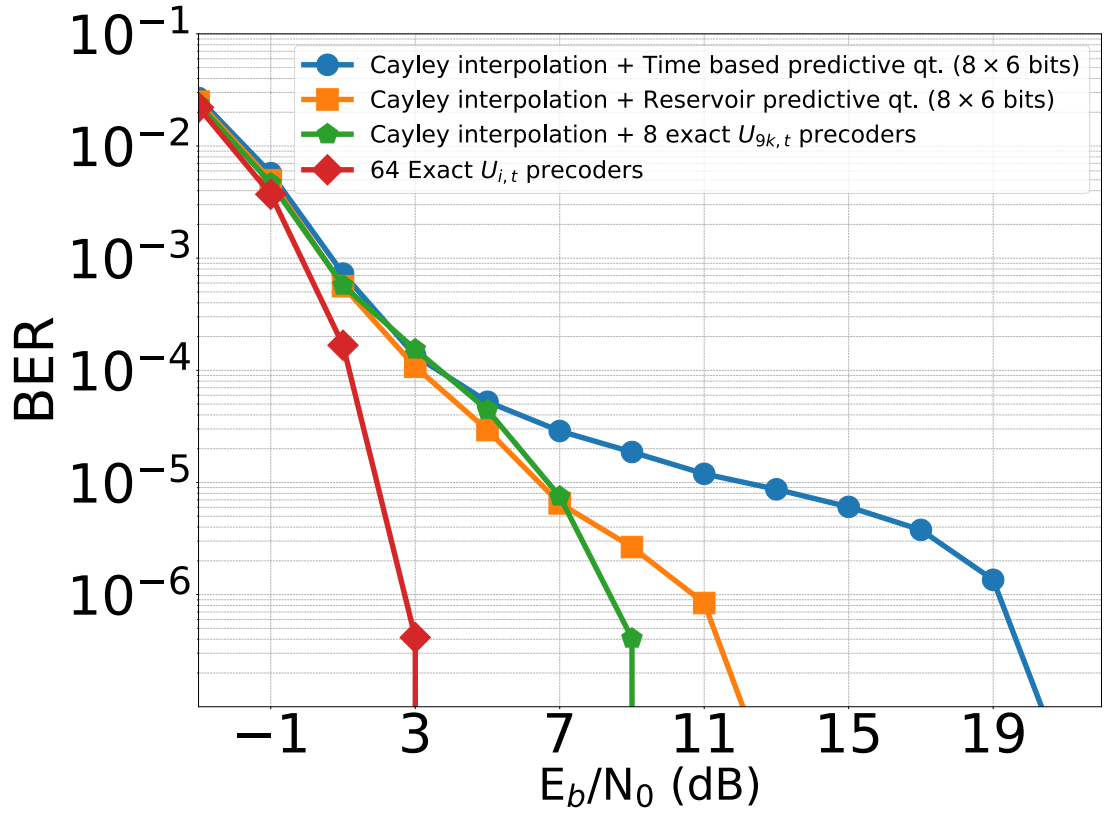

Figure 2.4: BER results: Here, red curve is the most ideal case considering exact $\mathbf{U}_{i,t}$ for all 64 subcarriers, at each time instant are available at the transmitter. The {green/yellow/blue} curves corresponds to the case in which $\{\mathbf{U}_{9k,t}/\tilde{\mathbf{U}}_{9k,t}$ from reservoir method/$\tilde{\mathbf{U}}_{9k,t}$ from [4]$\}$ is available for each time instant, and non fed back precoders are interpolated via Cayley method. Observe that the proposed framework BER curve provides significant improvement in $\mathrm{E_bN_0}$ levels over [4] (normalized Doppler $f_D T_s = 10^{-4}$).

We hypothesize that the key reason for the improved performance for both quantization error and BER in the reservoir computing approach, is the fact that f_P, q_P are coupled via the backward pass framework (explained towards the end of Section 2.3.4). Also, observe from Fig. 2.4 that the proposed framework BER curve (yellow) comes very close to the ideal 8 feedback curve (green). This can be explained due to the fact that the semi-unitary precoder basically rotates the data vector via its matrix transformation. For QPSK, we get some reasonable error margin for this rotation, which becomes more stringent as the simulated BER is reduced. Hence, we match the ideal curve for high BER region, and for low BER region, as the margin of error reduces, the curves diverge. For simulating the achievable rate, we quantize the sigma values ($\mathbf{\Sigma}_{i,t}$ from SVD of $\mathbf{H}_{i,t}$) using a 2 bit vector quantizer (k-means), and feed them back to the transmitter for fed back subcarriers ($\{9k, k \in \{0, 1, \ldots, 7\}\}$). For the non-fed back subcarriers, they are interpolated via a simple convex combination interpolation method as in [1]. Observe from Fig. 2.5 that the reservoir computing framework offers improvement in achievable rate for $f_D T_s = 10^{-4}$. Since the temporal variations for $f_D T_s = 10^{-2}, 10^{-1}$ are higher, the reservoir computing framework has to learn a faster-varying function, and hence the degradation in performance. However, it still matches the performance of the predictive quantizer in [4] for $f_D T_s = 10^{-2}$ and performs slightly better for $f_D T_s = 10^{-1}$.

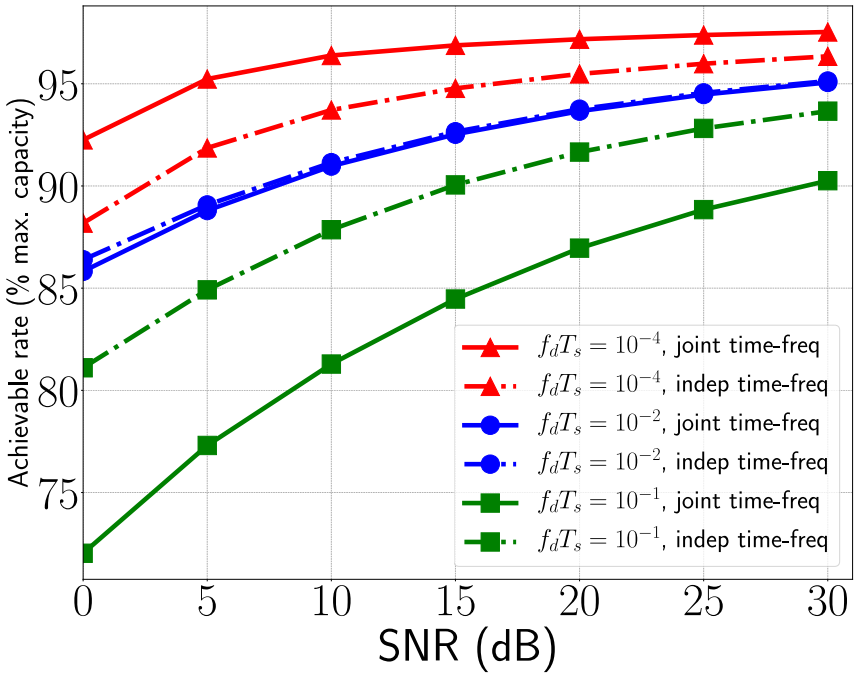

Figure 2.5: The results are presented as a percentage of the ideal achievable rate obtained when the transmitter has the accurate (unquantized) and non-interpolated estimates of $\mathbf{U}_{i,t}$ for each subcarrier and each time instant.

2.5 Conclusions and Future Work

In this paper, we have presented a reservoir computing framework for predictive quantization of SVD precoders by exploiting temporal correlations. The simulations reveal significant improvement in quantization error, BER, and achievable rate for IEEE Pedestrian-A channel model with normalized Doppler 10^{-4}. The novelty that enables these improvements lies in the training method for the reservoir framework, which refines the predicted coarse estimates as the reservoir evolves. The simulation results indicate that the proposed framework would be able to communicate at significantly lower power levels for the same BER, as illustrated in Fig. 2.4. Note that these results have been obtained by exploiting just the temporal correlations for predictive quantization, and can potentially improve if temporal-frequency correlations are exploited jointly. This motivates further study into the reservoir framework, and a detailed analysis of impact on performance caused by choice of different reservoir parameters like $\mathbf{A}$, $\tanh(\cdot)$, and D_{resv}.

Chapter 3

Backpropagation over the unitary group

Chapter Abstract

Backpropagation over scalar variables with scalar weights and activation functions is a widely studied algorithm and forms the backbone of many neural network architectures. To enable the search for the optimum interpolation function for the unitary precoding matrices in MIMO OFDM setting, we formulate the backpropagation algorithm over the unitary group, since here instead of learning functions of scalar variables, we needed to learn functions of unitary matrices. One thing centrally different in our approach from vanilla backpropagation schemes is that, the nodes, input/output and the weights are all unitary matrices, and not scalars. Due to this unitary structure in the problem considered, the algebra of gradients, convex combination schemes and standard activation functions needs to be tweaked. Since the unitary group is a lie group, i.e. it has both a group operation (multiplication) and a smooth manifold structure, indeed the above tweaks can be performed and backpropagation can be generalized to the unitary group. The following work summarizes the proposed backpropagation for unitary group.

3.1 Feed Forward Network

3.1.1 Architecture Considered

The unitary precoders $\mathbf{U}_i$ corresponding to subcarrier i is obtained by taking the SVD of $N_T \times N_R$ channel matrix $\mathbf{H}_i$, viz. $\mathbf{H}_i = \mathbf{U}_i\mathbf{\Sigma}_i\mathbf{V}_i$ (when $N_T \neq N_R$, full SVD should be taken instead of a compact SVD).

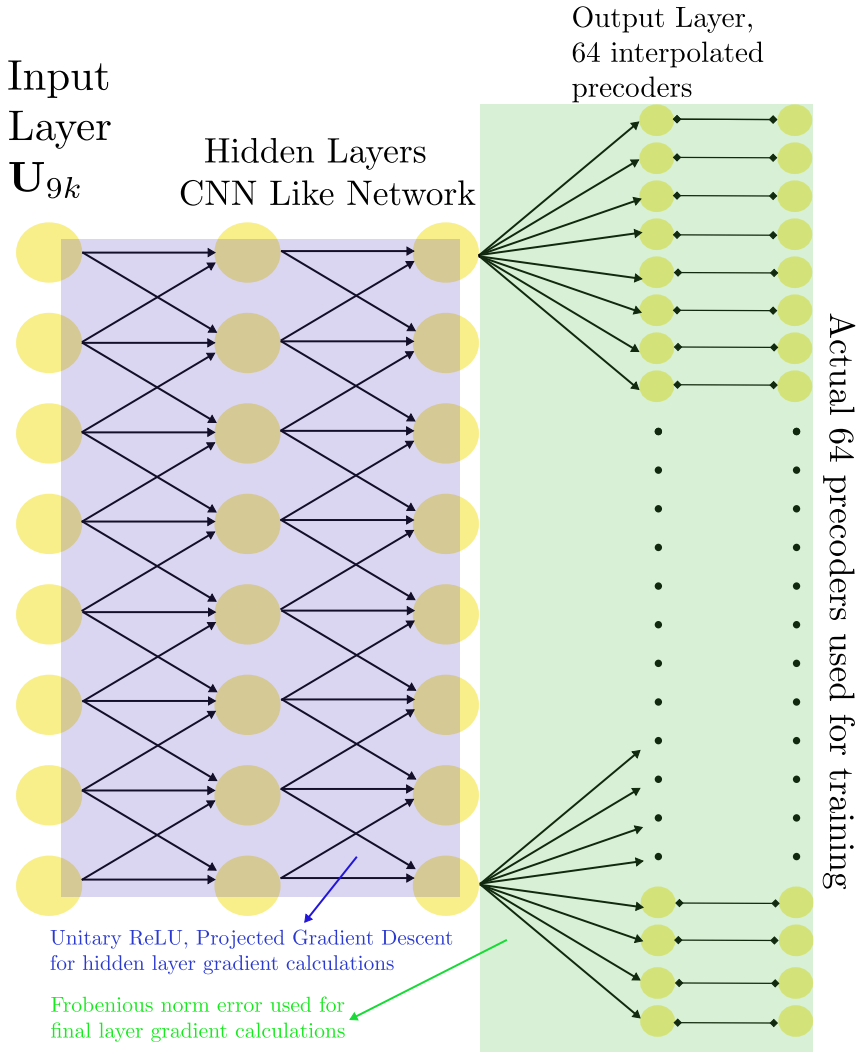

Figure 3.1: The proposed following NN architecture to learn the optimal interpolating f'n by observing precoder data arising from the channel for $\mathbf{U}_{9k,k\in\{0,1,\ldots 7\}} \rightarrow \mathbf{U}_{k,k\in\{0,1,\ldots 63\}}$

The architecture comprises of two types of layers. The first two layers resemble convolutional layers, and are motivated from the fact that the precoding matrix at a particular subcarrier is more correlated to it's neighbor subcarriers than other subcarriers. The last layer which maps the 8 matrices to 64 output matrices is a naive 'one to many layer' which multiplies the weight with the input to give the output.

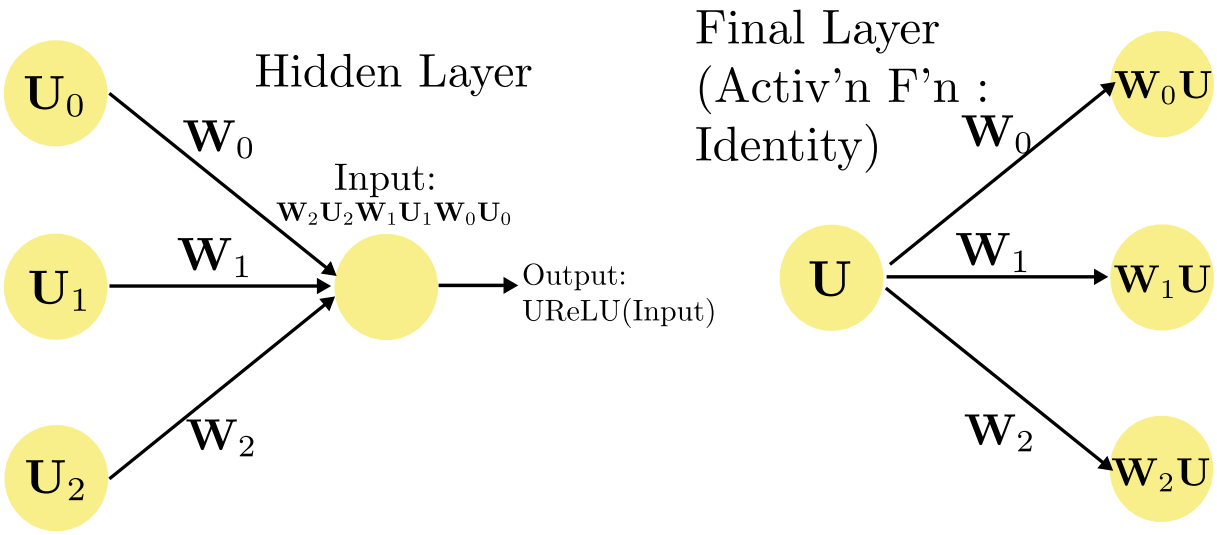

Figure 3.2: Convex Combination schemes in the network

3.1.2 Convex Combination schemes

Since the group operation on unitary manifold is multiplicative operation rather than addition, the convex combination scheme had to be altered to preserve the unitary structure of the nodes. The weights $\mathbf{W}_i$ are also unitary matrices.

3.1.3 Unitary ReLu function

The standard ReLu activation function was modified in the way given below to work on unitary manifolds:-

$$ReLU_{unitary}(k_+, k_-)(\mathbf{U}_{in}) = \begin{cases} expm(k_+ logm(\mathbf{U}_{in})); logm(\mathbf{U}_{in})) \text{ positive definite} \\ expm(k_- logm(\mathbf{U}_{in})); \text{ otherwise} \end{cases}$$

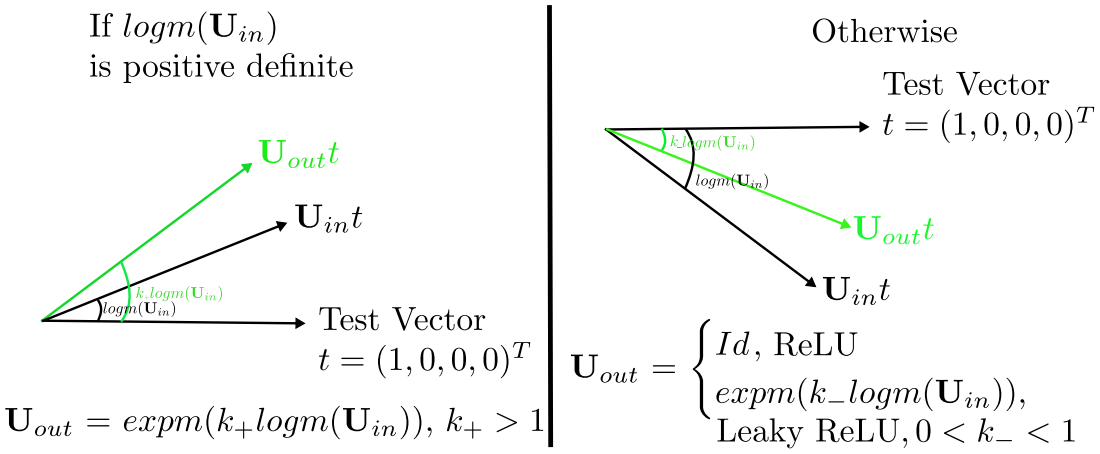

Figure 3.3: Unitary ReLU activation function: Pictorial Representation

- Unitary matrix acting upon a vector is analogous to the vector being rotated. Also, taking logm of Unitary matrix results in a skew hermitian matrix, which is analogous to $j\theta$ in $e^{j\theta}$
- Hence, if the rotation is in positive sense, the output of activation function is $expm(k_{+}logm(\mathbf{U}_{in}))$, where expm is matrix exponential, logm is matrix logarithm;
- If the rotation is in negative sense, the output of activation function is identity matrix (since the group operation being used is multiplication)
- A leaky ReLU can also be devised with a small slope (k_{-}, $k_{-} = 0$ for standard ReLU) if rotation is in negative sense, instead of the standard identity matrix

3.1.4 Concluding the Feed-Forward part

We now conclude the feed forward strategy for the tweaked backprop scheme. The network weights are initialized as random unitary matrices for the architecture in Fig. 3.1. Using Convex combination schemes in Section 3.1.2 the inputs to neurons are calculated. Each hidden layer neuron utilizes the Unitary ReLU activation function as discussed in Section 3.1.3. This is repeated till we get to the final layer. The final layer does not employ an activation function and the neuron output is simply neuron input itself.

3.2 Backpropagation & Gradient Calculations

3.2.1 Matrix Differentiation scheme

A roadblock towards the gradient calculations is the matrix by matrix derivative. The matrix by matrix derivative of $p \times q$ matrix $\mathbf{F}$ with respect to a $m \times n$ matrix $\mathbf{X}$ has the following form,

$$\frac{\partial \mathbf{F}}{\partial \mathbf{X}} = \begin{bmatrix} \frac{\partial \mathbf{F}}{\partial X_{1,1}} & \cdots & \frac{\partial \mathbf{F}}{\partial X_{1,n}} \\ \vdots & \ddots & \vdots \\ \frac{\partial \mathbf{F}}{\partial X_{m,1}} & \cdots & \frac{\partial \mathbf{F}}{\partial X_{m,n}} \end{bmatrix} \tag{3.1}$$

WLOG, consider that we perform backpropagation over 4×4 unitary matrices. Hence, both the weights and inputs/outputs are 4×4 as well. Thus, the gradient calculations will involve differentiating a 4×4 matrix with another 4×4 matrix, and the same will be used to update the weights, which are 4×4 themselves. However, the matrix by matrix derivative is 16×16 if we go with the traditional matrix by matrix derivative (3.1).

To solve this problem, we consider $\frac{\partial \mathbf{F}}{\partial \mathbf{X_{i,j}}}$ as the 4×4 matrix which indicates change in the i, j-th element of $\mathbf{X}$. Since we want the change in every element being considered, the required matrix would become $\sum_{i,j} \frac{\partial \mathbf{F}}{\partial \mathbf{X_{i,j}}}$. This is motivated by two observations:-

- Firstly, considering that we were backpropagating over just the element i,j. Then the required gradient would be $\frac{\partial \mathbf{F}}{\partial \mathbf{X_{i,j}}}$. Since we use the gradient to update the weight

matrix, subtracting this gradient to perform gradient descent would mean to make the i, j-th element more close to what is expected in the output.

- Secondly, if we consider a more basic first principles approach towards dealing with the problem, we would be do the following,

$$\frac{\partial(\mathbf{BAC})}{\partial \mathbf{A}} = \frac{B(A + h * \mathbb{1})C - BAC}{h}$$

where $\mathbb{1}$ is all ones matrix. This would reflect change in each element and give a 4*4 matrix as well.

- When doing the derivative of $\frac{\partial(\mathbf{BAC})}{\partial \mathbf{A}}$ in both the ways suggested above, we get the same derivative, which is $B\mathbb{1}C$

Hence, if we want back propagation over the whole matrix, summing over the entire entries would make sense, since the sum of individual i, j-th gradients will capture the gradient matrix representing the changes which should be done to get each i, j-th element modified appropriately to reduce the error function chosen. This can also be motivated by doing the things from first principle as suggested in the second approach.

3.2.2 Final Layer Gradient Calculations

The error function being used is the sum of squares of the frobenious norm difference between the output layer and the actual data. The gradient of frobenious norm squared with respect to the outputs is calculated in the way stated below.

$$\begin{aligned}
\frac{\partial \mathbf{E}}{\partial \sigma_{\mathbf{j}}^{\mathbf{L}}} &= \frac{\partial ||\sigma_{\mathbf{j}}^{\mathbf{L}} - \mathbf{o_j}||^{\mathbf{2}})}{\partial \sigma_{\mathbf{j}}^{\mathbf{L}}} \\
&= \frac{\partial \mathbf{Tr}((\sigma_{\mathbf{j}}^{\mathbf{L}} - \mathbf{o_j})(\sigma_{\mathbf{j}}^{\mathbf{L^H}} - \mathbf{o_j^H}))}{\partial \sigma_{\mathbf{j}}^{\mathbf{L}}} \\
&= \frac{\partial \mathbf{Tr}(\mathbf{I} + \mathbf{I} - \sigma_{\mathbf{j}}^{\mathbf{L}} \mathbf{o_j^H} - \mathbf{o_j} \sigma_{\mathbf{j}}^{\mathbf{L^H}})}{\partial \sigma_{\mathbf{j}}^{\mathbf{L}}} \\
&= -(\frac{\partial \mathbf{Tr}(\sigma_{\mathbf{j}}^{\mathbf{L}} \mathbf{o_j^H})}{\partial \sigma_{\mathbf{j}}^{\mathbf{L}}} + \frac{\partial \mathbf{Tr}(\mathbf{o_j} \sigma_{\mathbf{j}}^{\mathbf{L^H}})}{\partial \sigma_{\mathbf{j}}^{\mathbf{L}}}) \\
&= -2 * o_j
\end{aligned} \tag{3.2}$$

Here $\mathbf{E}$ represents the error function, σ_j^L represents the j-th final layer output o_j represents the j-th expected output the network is being trained against, We use the identities $\frac{\partial \mathbf{Tr(AXB)}}{\partial \mathbf{X}} = A^T B^T$ and $\frac{\partial \mathbf{Tr(AX^TB)}}{\partial \mathbf{X}} = BA$ to simplify the second last equation.

This calculation sets up the gradient descent scheme. Since, this gradient is with respect to outputs of layer L, to update the weights between layer L-1 and layer L, we need the gradient wrt to the weights, for which chain rule is used.

$$\begin{aligned}\frac{\partial \mathbf{E}}{\partial \mathbf{w_{ij}}} &= -\frac{\partial \mathbf{E}}{\partial \sigma_{\mathbf{j}}^{\mathbf{L}}}\frac{\partial \sigma_{\mathbf{j}}^{\mathbf{L}}}{\partial \mathbf{w_{ij}}} \\ &= -2 * o_j * \frac{\partial(\mathbf{w_{ij}} * \mathbf{X-1})}{\partial \mathbf{w_{ij}}} \\ &= -2 * o_j * \mathbb{1} * X_{-1}\end{aligned} \tag{3.3}$$

where X_{-1} is the appropriate penultimate output corresponding to i,j. (Recall the final layer scheme, which doesn't use any activation function). Once gradients wrt weights are calculated, the weights are updated by using projected gradient descent:-

$$w_{ij} = closest\_unitary(w_{ij} - \eta\frac{\partial \mathbf{E}}{\partial \mathbf{w_{ij}}}) \tag{3.4}$$

where closest_unitary(.) maps the input to the closest matrix in the unitary group.

The gradient wrt to the output ($-\frac{\partial \mathbf{E}}{\partial \sigma_{\mathbf{j}}^{\mathbf{L}}}$) is backpropagated to enable calculation of gradients of the hidden layers.

3.2.3 Hidden Layer Gradient Calculations

.

1. Using the gradient wrt final layer output and chain rule, gradient wrt penum layer output is calculated by summing over the connected next layer nodes

$$\frac{\partial \mathbf{E}}{\partial \sigma_{\mathbf{j}}^{\mathbf{L-1}}} = \sum_{k \in connected\_nodes} \frac{\partial \mathbf{E}}{\partial \mathbf{sum_k^L}}\frac{\partial \mathbf{sum_k^L}}{\partial \sigma_{\mathbf{j}}^{\mathbf{L-1}}}$$

   where sum_k^L is the input to kth neuron of layer L such that jth node of layer L-1 is connected to kth node of layer L. Recall from section 3.1.2 that we have an expression for sum_k^L in terms of its connected nodes output σ_j^{L-1} and their respective weights.

2. Since all layers apart from final layer use the Unitary ReLU activation function, the gradient wrt output is converted to gradient wrt input by differentiating the Unitary ReLU. The gradient wrt 'layer input' is then backpropagated for calculation of previous layer gradients similar to what was done with gradient of the final layer weights.

$$\frac{\partial \mathbf{E}}{\partial \mathbf{sum_j^{L-1}}} = \frac{\partial \mathbf{E}}{\partial \sigma_{\mathbf{j}}^{\mathbf{L-1}}}\frac{\partial \sigma_{\mathbf{j}}^{\mathbf{L-1}}}{\partial \mathbf{sum_j^{L-1}}}$$

   where $\frac{\partial \sigma_{\mathbf{j}}^{\mathbf{L-1}}}{\partial \mathbf{sum_j^{L-1}}}$ is just the derivative of the unitary ReLU since $\sigma_j^{L-1} = ReLU_{unitary}(sum_j^{L-1})$

3. To get gradient wrt weights of the previous layers, each of the input is differentiated one by one wrt weights and then multiplied with gradient wrt input to get gradient wrt weights, which is then used for Projected Gradient descent to update the weights

$$\frac{\partial \mathbf{E}}{\partial \mathbf{w_{ij}}} = \frac{\partial \sigma_{\mathbf{j}}^{\mathbf{L-1}}}{\partial \mathbf{sum}_{\mathbf{j}}^{\mathbf{L-1}}} \frac{\partial \mathbf{sum}_{\mathbf{j}}^{\mathbf{L-1}}}{\partial \mathbf{w_{ij}}}$$

where i denotes the index of nodes in layer L-2 connected to jth node of layer L-1. The weights are updated similar to last layer weights using the projected gradient scheme (3.4).

Steps 1,2,3 are repeated till the first layer (the input layer is reached) and all the weights are updated using (3.4).

3.3 Regularization Procedure

Recall the 'unitary matrix rotates a vector' analogy discussed in 3.1.3. This analogy also helps us to formulate a regularization scheme. Regularization is done by imposing a penalty upon deviation of weights from identity matrix, as it is not good for the weights to rotate vectors by a lot and hence overfit.
Thus, the term $expm(\lambda logm(U))$ is multiplied to the gradient for regularization. If the matrix U is close to identity, the regularization term will also be close to identity and not affect the gradient by much. Hence the modified update rule becomes :-

$$w_{ij} = closest\_unitary(w_{ij} - \eta \frac{\partial \mathbf{E}}{\partial \mathbf{w_{ij}}} expm(\lambda logm(w_{ij})))$$

Bibliography

[1] A. Gupta, K. Appaiah, and R. Vaze, "Predictive quantization and joint Time-Frequency interpolation technique for MIMO-OFDM precoding," in *IEEE ICC'19 - WC Symposium*, Shanghai, P.R. China, May 2019.

[2] D. J. Love, R. W. Heath, V. K. Lau, D. Gesbert, B. D. Rao, and M. Andrews, "An overview of limited feedback in wireless communication systems," *IEEE Journal on Selected Areas in Communications*, vol. 26, no. 8, 2008.

[3] N. Khaled, B. Mondal, R. W. Heath, G. Leus, and F. Petré, "Quantized multi-mode precoding for spatial multiplexing MIMO-OFDM systems," in *IEEE 62nd Vehic. Technol. Conf.*, vol. 2. IEEE, 2005, pp. 867–871.

[4] S. Schwarz and M. Rupp, "Predictive Quantization on Stiefel Manifold," *IEEE Signal Processing Letters*, vol. 22, no. 2, pp. 234–238, Feb 2015.

[5] S. Schwarz, R. W. Heath, and M. Rupp, "Adaptive Quantization on a Grassmann-Manifold for Limited Feedback Beamforming Systems," *IEEE Transactions on Signal Processing*, vol. 61, no. 18, pp. 4450–4462, Sept 2013.

[6] R.-A. Pitaval, A. Srinivasan, and O. Tirkkonen, "Codebooks in flag manifolds for limited feedback mimo precoding," 01 2013, pp. 1–5.

[7] K. Schober, R. Pitaval, and R. Wichman, "Improved User-Specific Channel Estimation Using Geodesical Interpolation at the Transmitter," *IEEE Wireless Communications Letters*, vol. 4, no. 2, pp. 165–168, April 2015.

[8] R. T. Krishnamachari and M. K. Varanasi, "On the geometry and quantization of manifolds of positive semi-definite matrices," *IEEE Transactions on Signal Processing*, vol. 61, no. 18, pp. 4587–4599, 2013.

[9] C.-B. Chae, D. Mazzarese, N. Jindal, and R. W. Heath, "Coordinated beamforming with limited feedback in the MIMO broadcast channel," *IEEE Journal on Selected Areas in Communications*, vol. 26, no. 8, 2008.

[10] Y. Chou and T. Sang, "Efficient interpolation of precoding matrices in MIMO-OFDM systems," in *SPAWC, 2010*, June 2010, pp. 1–4.

[11] D. Sacristán-Murga and A. Pascual-Iserte, "Differential feedback of MIMO channel Gram matrices based on geodesic curves," *IEEE Transactions on Wireless Communications*, vol. 9, no. 12, pp. 3714–3727, 2010.

[12] T. Li, F. Li, and C. Li, "Manifold-based predictive precoding for the time-varying channel using differential geometry," *Wireless Networks*, vol. 22, no. 8, pp. 2773–2783, Nov 2016.

[13] Y. Li, S. Zhu, H. Tong, and M. Xu, "Enhanced limited rate implicit CSI feedback and its usage in covariance matrix based MU-MIMO," in *WCNC, 2013*. IEEE, 2013, pp. 3067–3071.

[14] Y. Jeon, H. Kim, Y. Cho, and G. Im, "Time-Domain Differential Feedback for Massive MISO-OFDM Systems in Correlated Channels," *IEEE Transactions on Communications*, vol. 64, no. 2, pp. 630–642, Feb 2016.

[15] S. Schwarz and M. Rupp, "Adaptive channel direction quantization for frequency selective channels," in *2012 Proceedings of the 20th European Signal Processing Conference (EUSIPCO)*. IEEE, 2012, pp. 2536–2540.

[16] K. A. Krakowski, L. Machado, F. S. Leite, and J. Batista, "A modified Casteljau algorithm to solve interpolation problems on Stiefel manifolds," *J. of Comp. and Appl. Math.*, vol. 311, pp. 84–99, 2017.

[17] A. Edelman, T. A. Arias, and S. T. Smith, "The geometry of algorithms with orthogonality constraints," *SIAM journal on Matrix Analysis and Applications*, vol. 20, no. 2, pp. 303–353, 1998.

[18] R. Pitaval and O. Tirkkonen, "Joint Grassmann-Stiefel Quantization for MIMO Product Codebooks," *IEEE Transactions on Wireless Communications*, vol. 13, no. 1, pp. 210–222, January 2014.

[19] R. Chakraborty and B. C. Vemuri, "Statistics on the (compact) Stiefel manifold: Theory and Applications," *CoRR*, vol. abs/1708.00045, 2017. [Online]. Available: http://arxiv.org/abs/1708.00045

[20] T. Inoue and R. W. Heath, "Grassmannian predictive coding for limited feedback multiuser MIMO systems," in *ICASSP*, 2011, pp. 3076–3079.

[21] S. Fiori, T. Kaneko, and T. Tanaka, "Mixed maps for learning a Kolmogoroff-Nagumo-type average element on the compact Stiefel manifold," in *ICASSP, 2014*, May 2014, pp. 4518–4522.

[22] V. Saxena, https://github.com/vidits-kth/py-itpp.

[23] J. Chang, I.-T. Lu, and Y. Li, "Adaptive codebook based channel prediction and interpolation for multiuser mimo-ofdm systems," in *2011 International Conference on Communications (ICC)*. IEEE, pp. 1–5.

[24] H. Jaeger and H. Haas, "Harnessing nonlinearity: Predicting chaotic systems and saving energy in wireless communication," *science*, vol. 304, no. 5667, pp. 78–80, 2004.

[25] A. Jalalvand, G. Van Wallendael, and R. Van de Walle, "Real-time reservoir computing network-based systems for detection tasks on visual contents," in *2015 7th International Conference on Computational Intelligence, Communication Systems & Networks*. IEEE, pp. 146–151.

[26] S. Mosleh, L. Liu, C. Sahin, Y. R. Zheng, and Y. Yi, "Brain-inspired wireless communications: Where reservoir computing meets mimo-ofdm," *IEEE transactions on neural networks and learning systems*, no. 99, pp. 1–15, 2017.

[27] J. Pathak, Z. Lu, B. R. Hunt, M. Girvan, and E. Ott, "Using machine learning to replicate chaotic attractors and calculate lyapunov exponents from data," *Chaos: An Interdisciplinary Journal of Nonlinear Science*, vol. 27, no. 12, p. 121102, 2017.

[28] D. Verstraeten, B. Schrauwen, D. Stroobandt, and J. Van Campenhout, "Isolated word recognition with the liquid state machine: a case study," *Information Processing Letters*, vol. 95, no. 6, pp. 521–528, 2005.

[29] R. Shafin, L. Liu, J. Ashdown, J. Matyjas, M. Medley, B. Wysocki, and Y. Yi, "Realizing green symbol detection via reservoir computing: An energy-efficiency perspective," in *2018 IEEE International Conference on Communications (ICC)*. IEEE, 2018, pp. 1–6.